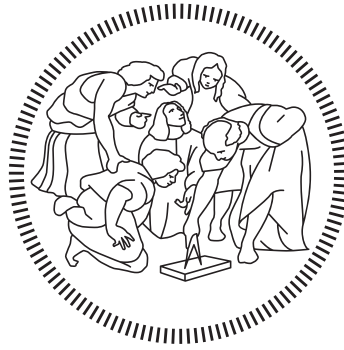


POLITECNICO DI MILANO  
Scuola di Ingegneria Industriale e dell'Informazione  
Corso di Laurea Magistrale in Rotary Wing Aircraft



# Whirl flutter stability enhancement by rotor twist optimization

**Advisor:** Prof. Giuseppe Quaranta  
**Co-Advisor:** Vincenzo Muscarello

**Thesis by:**  
Andrea Bonetti ID: 904719

Academic Year 2019–2020

---

---

*To my grandpa Tonio,  
that leave us too early.*

---

# Acknowledgments

I would like to thank my family, especially my parents, who supported and encouraged me on this journey, and allowed me to be able to reach this goal. Thanks to my lifelong friends and the new ones known during these years, for the help and support given to me during this experience. Finally, further thanks goes to my advisors Giuseppe Quaranta and Muscarello Vincenzo for having offered me this interesting work and the help given to me.



# Abstract

Nowadays whirl flutter is one of the major challenge for the development of tilt-rotor aircraft, due to the fact that this instability limiting strongly the forward flight velocity for this kind of aircrafts. To avoid this problem the current solution is to use rigid and thick wings in order to increase the torsional stiffness. Consequently the thesis purpose is to improve the whirl flutter velocity, acting on two different parameters: the wing structure and the rotor blade twist. Variations on the rotor blade twist are able to improve the whirl flutter stability, generating an increase in the required power. To maintain the power unchanged, the thickness of the wings is modified, this changes the torsional stiffness value, but in turn also the drag produced. In this way, it is possible to find an optimal configuration that can increase stability, leaving the maximum power unchanged.

Basing on a detailed model of the Bell XV-15, modal and aerodynamic analysis, changing the wing thickness are done, in order to obtain the necessary parameters for the stability analysis in CAMRAD/JA. An optimization process is made to generate optimal solutions that combine thick and blade twist variation capable of improving the whirl flutter velocity without increase the required power. On the best solutions, trim and loads results are investigated in order to study the effects of variations. Finally, the best solutions are analysed in different condition, trim with a maximum power limit and in helicopter configuration, to show the effects on aircraft performance in a different trim condition. The results shown that with blade twist modification is possible to obtain an optimal wing thickness able to improve the whirl flutter velocity, maintaining the same power plant.

**Keywords:** Aeroelasticity, Whirl flutter, Tilt rotor, Blade twist, Thick to chord ratio





# Sommario

Attualmente, l'instabilità aerodinamica chiamata whirl flutter, rappresenta una delle sfide più ardue nello sviluppo e nella diffusione del tilt-rotor, perché questa stessa impone delle forti limitazioni sulle prestazioni del velivolo in fase di volo rettilineo. Per eliminare questo problema, la soluzione attualmente utilizzata è quella di impiegare nel velivolo ali con elevato spessore, in modo da irrigidire la struttura ed evitare le instabilità. Sulla base di questa riflessione, l'obiettivo della tesi è quello di incrementare la velocità limite imposta dal whirl flutter, andando ad agire su due diversi parametri: la struttura dell'ala e lo svergolamento delle pale del rotore. Lo svergolamento delle pale è in grado di influire sul limite di stabilità del whirl flutter, causando però un aumento della potenza richiesta. Per mantenere la potenza inalterata, si va ad agire sullo spessore delle ali, questo modifica il valore di resistenza torsionale, ma a sua volta anche la resistenza prodotta. In questo modo, si cerca di trovare una configurazione ottimale che possa incrementare la stabilità, lasciando invariata la potenza massima.

Utilizzando come riferimento il velivolo sperimentale Bell XV-15, sono state fatte diverse analisi modali e aerodinamiche al variare del valore dello spessore, in modo da ottenere i parametri richiesti per l'analisi di stabilità in CAMRAD/JA. Attraverso un processo di ottimizzazione, si cerca di ottenere la soluzione ottimale, che incrementi la velocità di whirl flutter senza aumentare la potenza, combinando al meglio la variazione nello spessore delle ali con lo svergolamento delle pale del rotore. Sulle soluzioni ottimali ottenute, si analizzano i valori di trim e dei carichi, in modo da valutare gli effetti prodotti dalle modifiche effettuate. Infine, sulle soluzioni ottimali vengono effettuate due ulteriori analisi, una a potenza massima fissata e una in modalità elicottero, per verificare gli effetti delle modifiche in due diverse condizioni di funzionamento.

I risultati ottenuti mostrano come attraverso la modifica nella legge di svergolamento delle pale del rotore sia possibile trovare uno spessore delle ali in grado di incrementare il limite di stabilità del whirl flutter, mantenendo inalterato il valore di potenza massima erogabile dal motore.

**Parole chiave:** Aeroelasticità, Whirl flutter, Tilt rotor, Svergolamento della pala, rapporto spessore corda



# Contents

Acknowledgments	I
Abstract	III
Sommario	V
List of figures	IX
List of tables	XI
Nomenclature	XIII
Introduction	1
<b>1 Tilt-rotor</b>	<b>3</b>
1.1 Tilt-rotor operation . . . . .	3
1.2 Whirl Flutter . . . . .	4
1.2.1 Phenomena Description . . . . .	4
<b>2 Model description</b>	<b>9</b>
2.1 Normal Modes . . . . .	10
2.2 Aerodynamics . . . . .	14
<b>3 Optimization scheme</b>	<b>21</b>
3.1 Optimization Algorithm . . . . .	21
3.2 Optimization structure . . . . .	22
<b>4 Rotor twist optimization</b>	<b>25</b>
4.1 Reference Case . . . . .	25
4.2 Optimization Procedure . . . . .	28
4.3 Optimization Results . . . . .	28
4.3.1 Single slope case . . . . .	31
4.3.2 Two slope case . . . . .	31
4.3.3 Three slope case . . . . .	35

4.3.4	Trim and Loads . . . . .	41
4.4	Power limitation . . . . .	43
4.5	HEMODE Analysis . . . . .	49
<b>Conclusions</b>		<b>53</b>

# List of Figures

1.1	Examples of modern Tilt-rotor in different flight configuration . . .	3
1.2	Propeller-Nacelle model (from [12]) . . . . .	5
1.3	Natural vibration modes of system (from [12]) . . . . .	6
1.4	Aerodynamic forces and moments on a pitching and plunging propeller at zero thrust (from [12]) . . . . .	7
1.5	Rotor blade deformations due to the bending (from [12]) . . . . .	8
2.1	Bell XV-15 . . . . .	9
2.2	Nastran Finite-Element Model . . . . .	11
2.3	Single cell torque box . . . . .	12
2.4	Torsional stiffness trend respect thickness . . . . .	13
2.5	XV-15 Model for the Aerodynamic Analysis in XFRL5 . . . . .	15
2.6	Wind tunnel values for $M = 0.4$ compared with the aerodynamic coefficients at the same speed reconstructed from low speed wind tunnel values . . . . .	16
2.7	Aerodynamic coefficients for $M = 0.1$ from Xfrl5 respect real values	17
2.8	Aerodynamic coefficients for $M = 0.5$ from Xfrl5 respect real values	17
2.9	Aerodynamic coefficients for $M = 0.6$ from Xfrl5 respect real values	18
2.10	Behaviour of aerodynamic coefficients for different thickness values - $M = 0.2$ . . . . .	19
3.1	Optimization procedure scheme . . . . .	23
4.1	Linear regression and real blade twist distribution . . . . .	26
4.2	Whirl-mode frequency and damping w.r.t. flight speed - Symmetric roots . . . . .	26
4.3	Whirl-mode frequency and damping w.r.t. flight speed - Antisymmetric roots . . . . .	27
4.4	Whirl modes damping variation changing the $t/c$ . . . . .	30
4.5	Solution 3 - Twist distribution . . . . .	32
4.6	Solution 3: Whirl-mode frequency and damping w.r.t. flight speed - Symmetric roots . . . . .	33
4.7	Solution 3: Whirl-mode frequency and damping w.r.t. flight speed - Antisymmetric roots . . . . .	34

4.8	Solution 16 - Twist distribution . . . . .	35
4.9	Solution 16: Whirl-mode frequency and damping w.r.t. flight speed - Symmetric roots . . . . .	36
4.10	Solution 16: Whirl-mode frequency and damping w.r.t. flight speed - Antisymmetric roots . . . . .	37
4.11	Solution 21 - Twist distribution . . . . .	38
4.12	Solution 21: Whirl-mode frequency and damping w.r.t. flight speed - Symmetric roots . . . . .	39
4.13	Solution 21: Whirl-mode frequency and damping w.r.t. flight speed - Antisymmetric roots . . . . .	40
4.14	Trim results . . . . .	41
4.15	Rotor loads and coning angle . . . . .	42
4.16	Bending and Control moments (mean component) w.r.t. flight speed	42
4.17	One slope Solution : whirl-mode damping w.r.t. flight speed - Fixed power . . . . .	44
4.18	Two slopes Solution : whirl-mode damping w.r.t. flight speed - Fixed power . . . . .	45
4.19	Three slopes Solution : whirl-mode damping w.r.t. flight speed - Fixed power . . . . .	45
4.20	Trim results - Fixed power . . . . .	46
4.21	Rotor loads and coning angle - Fixed power . . . . .	47
4.22	Bending and Control moments (mean component) w.r.t. flight speed - Fixed power . . . . .	48
4.23	HEMODE - Trim results . . . . .	49
4.24	HEMODE - Thrust distribution in hovering . . . . .	50
4.25	HEMODE - Coning angle and Bending moment (mean component) w.r.t. flight speed . . . . .	51
4.26	HEMODE - Control moment (mean component) and Figure of merit w.r.t. flight speed . . . . .	51

# List of Tables

2.1	XV-15 Basic Information . . . . .	10
2.2	Graphite-epoxy material properties . . . . .	11
2.3	Wing properties from Acree's reference . . . . .	12
2.4	Aerodynamic Surface Data from real XV-15 . . . . .	14
2.5	Parameters for XFRL5 analysis . . . . .	16
4.1	Reference Solution . . . . .	27
4.2	Optimization Results . . . . .	29
4.3	Sol 3 - results summary . . . . .	31
4.4	Sol 16 - results summary . . . . .	32
4.5	Sol 21 - results summary . . . . .	38
4.6	Lycoming LTC1K-41K turboshaft engine (modified T53L13B) - Power ratings . . . . .	43
4.7	Stability limit - Unlimited power w.r.t. Fixed Power . . . . .	43





# Nomenclature

$\beta_{trim}$	Trim coning angle
$\Gamma$	Dihedral angle
$\gamma$	Rotor lock number
$\Lambda$	Sweep angle
$\Omega$	Rotor rotating speed
$\sigma$	Rotor solidity
$\theta_{tw_0}$	Baseline twist slope
$\theta_{tw_1}/\theta_{tw_0}$	Twist slope ratio - First segment
$\theta_{tw_2}/\theta_{tw_0}$	Twist slope ratio - Second segment
$\theta_{tw_3}/\theta_{tw_0}$	Twist slope ratio - Third segment
$AoA$	Angle Of Attack
$AR$	Aspect Ratio
$AWB$	Antisymmetric Wing Bending mode
$AWC$	Antisymmetric Wing Chord mode
$AWT$	Anrismatic Wing Torsion mode
$b$	Wing span
$c$	Aerodynamic chord
$C_D$	Drag coefficient
$C_L$	Lift coefficient
$FM$	Figure of Merit

*ISA* International Standard Atmosphere

$K_\theta$  Torsional stiffness

$P_0$  Baseline required power

$P_{MAX}$  Maximum engine(s) power

$R$  Rotor radius

$r/R$  Radial station

$Re$  Reynolds number

$S$  Wing area

*SWB* Symmetric Wing Bending mode

*SWC* Symmetric Wing Chord mode

*SWT* Symmetric Wing Torsion mode

$t/c$  Thick to chord ratio

$V_m$  Dive velocity

$V_{MAX}$  Maximum flight speed

$V_{wf_0}$  Baseline whirl flutter velocity

$V_{wf}$  Whirl flutter velocity

$W_{TO}$  Gross Take-off weight

# Introduction

Vertical take off and landing aircraft (VTOL) represent one of the most challenging types of aircraft to be designed. The tilt-rotor configuration is particularly challenging due to the tilting of nacelles and rotors. In particular one of the hardest challenges is to reach the performance similar to a turboprop in terms of forward flight velocity. The strongest limitation is imposed by the whirl flutter, an aeroelastic instability that occurs at high speed, due to the unsteady aerodynamic loads introduced by the rotating propeller. Therefore, the presence of tilting rotor at the wing tips, which makes this aircraft so special and versatile, is at the same time a limiting factor for its forward flight performance.

Many studies have been conducted on whirl flutter to investigate its nature and which parameters influence it, in order to find possible approaches to increase the boundary imposed on the maximum forward flight velocity. Numerous approaches have been investigated: tailored-stiffness wing [11, 10], active stability augmentation [3], variable geometry rotors [8], highly swept tips [13] and folding rotors [4]. An alternative approach is provided by Acree [1], who showed that by rearward offsets of the aerodynamic-center of the rotor blade with respect to the elastic axis or forward offsets of the blade center of gravity, it is possible to obtain an increase of the stability margin. So, up to now all investigated solutions, more or less, increase the stability limit due to the whirl flutter, however they often require an increase of power, weight and/or complexity. In this work a different approach to improve the whirl flutter stability is followed, changing the rotor blade twist as done in Ref. [9]. The results obtained through a preliminary analysis show that using a linear blade twist law, and reducing its slope with respect to the original value, it is possible to increase the whirl flutter stability. By decreasing the slope of the twist law, the effect is to change the thrust per unit of length, moving the total thrust force towards the blade tip. This change also causes an increase in the bending moment towards the root of the blade and an increase in the trim coning angle,  $\beta_{trim}$ . A positive trim coning angle, also generates a positive pitch-lag coupling (positive for lag back, pitch down), improving the stability limits of the whirl flutter. Generally for the proprotor in cruise the trim coning angle is negative, consequently also pitch-lag coupling is negative, which limits the speed of the whirl flutter. Therefore the increase of the coning angle due to the decrease of blade twist slope, allows to obtain a positive  $\beta_{trim}$ , which as mentioned

before improves the stability margin. However, the higher thrust forces on the blade tip section, due to the higher lift, also returns an higher local induced drag, increasing the power required. Adverse effects occur for the case in which the slope increases, the stability limit is reduced, due to the thrust that moves away from the tip, reducing the  $\beta_{trim}$  value, which in turn reduces the positive effects of pitch-lag coupling. in conclusion, by reducing the slope of the twist law, it is possible to improve the stability limit of the whirl flutter, while at the same time increasing the power required. Consequently it is necessary to find the optimal trade off that leads to the best overall performance for the aircraft.

## Thesis Purpose and Structure

The thesis purpose is to use the blades twist approach to increase the stability limit of whirl flutter and compensate the possible increase of power due to the twist modification reducing the power absorbed by other parts, keeping the available power unchanged. To do it, the idea is to modify the wing thickness, because to reach a sufficiently high whirl flutter resistance, it is necessary to increase the wing torsional stiffness. However this in turn limits the cruise efficiency due to high drag forces. Considering the thick to chord ratio ( $t/c$ ) of the wing airfoil, it is possible to verify if an optimal trade off configuration can be found.

The structure of this work is organized as follow:

- **chapter 1:** tilt-rotor operation and brief discussion of the Whirl Flutter phenomena;
- **chapter 2:** model presentation and detailed description of modification due to the  $t/c$  variation;
- **chapter 3:** presentation of the optimization algorithm;
- **chapter 4:** presentation of the results.

# Chapter 1

## Tilt-rotor

The tilt-rotors are very interesting aircraft design, because combine the positive aspects of helicopters, vertical take-off and hover, with the flight quality and forward speed close to a conventional turboprop. This chapter briefly introduces the operation of the tilt-rotor and in the following section it introduces from a theoretical point of view the whirl flutter problem.

### 1.1 Tilt-rotor operation



(a) Leonardo Helicopter AW609



(b) Bell V280

Figure 1.1: Examples of modern Tilt-rotor in different flight configuration

Tilt-rotor is an hybrid between conventional helicopter and turboprop aircraft: it presents on the wing tip a rotating nacelle with a rotor similar to a helicopter one. For the vertical take-off, nacelles are perpendicular to the fixed wing plane: this configuration is the helicopter mode (HEMODE). After the take-off, when the aircraft starts to increase the speed, rotors are progressively tilted forward, until they reach the horizontal position. This is the airplane mode (APMODE), where

the lift is provided only by the wing and rotor produces only the thrust. APMODE allows to avoid the problem of stall on retreating blade and other problems relates to the conventional helicopters.

## 1.2 Whirl Flutter

The position and the degrees of freedom of the rotor, generates strong vibratory phenomena during forward flight that affects the performance of the tilt-rotor, in some cases, called whirl flutter.

Whirl flutter is an aeroelastic phenomenon that may occur in a flexibly mounted engine and rotor system. The degrees of freedom and loads introduced by the engine's rotating masses and the interference in flow field generated by the propeller itself may cause an unsymmetrical distribution of the lift force on the transversely vibrating propeller, that is the principle cause of this kind of instability. So this phenomenon relates the deformation and forces of the aircraft during forward flight with the effects of a rotating rotor. Whirl flutter may cause the rotor mounting to have unstable vibrations or even to failure of the engine, nacelle or whole wing. For these reasons, this phenomenon is extremely dangerous, especially for the tilt-rotor, because the nacelles are installed on the wing tips, a very sensitive area from the aeroelastic point of view.

So the whirl flutter represent a stronger limitation for the tilt-rotor performance, because the stability limit imposed by it is a constraint for the forward speed.

### 1.2.1 Phenomena Description

To explain whirl flutter, an idealized propeller-nacelle model as been introduced, as shown in **Figure 1.2**. A simple cantilever beam with uniform mass and stiffness property, represent the nacelle structure, and two rotational spring located between the rotor and the pivot point, simulate the wing flexibility.

For this idealized system the equations of motion may be derived using Lagrange's dynamic equations:

$$\begin{cases} I_n \ddot{\theta} + C_\theta \dot{\theta} + K_\theta \theta - I_x \Omega \dot{\phi} & = aRL_z + M_y \\ I_x \Omega \dot{\theta} + I_n \ddot{\phi} + C_\phi \dot{\phi} - K_\phi \phi & = aRL_y + M_z \end{cases} \quad (1.1)$$

where  $I_n$  is the pylon angular moment of inertia respect the pivot point,  $I_x$  is the polar moment of inertia of the rotor,  $C_{(\cdot)}$  and  $K_{(\cdot)}$  are, respectively, the damping and the stiffness of both degree of freedom. In the right side there are  $L_{(\cdot)}$  that represents the total aerodynamic force due to the propeller in the respectively direction, and  $M_{(\cdot)}$  is the total aerodynamic moment due to the propeller around the respectively axes. Note that differently from the usual dynamic terms, the spinning propeller introduce gyroscopic and aerodynamics terms. Gyroscopic forces play an important role, because they create a coupling between the natural

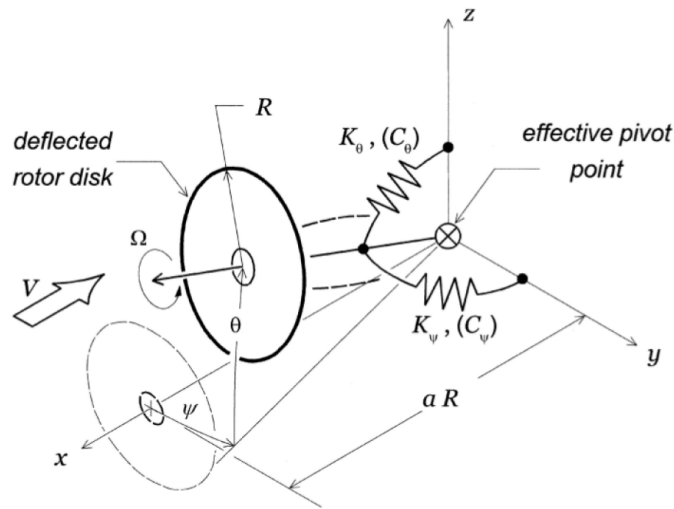


Figure 1.2: Propeller-Nacelle model (from [12])

vibration modes and the propeller action.

The natural modes of the system are then characterized by whirl or precession modes, that are described in the center draw in the **Figure 1.3**.

The higher frequency mode is defined as forward whirl mode, which is associated with a whirl of the hub in the direction of propeller rotation. Similarly, the lower frequency mode is defined as the backward whirl mode, associated with a whirl in the opposite direction of the propeller rotation. Whirl modes produce an angle of attack (AoA) variation on the blade element of the propeller, which in turn generates an aerodynamic force variation, which provides the mechanism for instability.

This kind of instability, for rigid blade systems, occurs in the backward whirl mode, instead for propeller with very flexible blade or equipped with flap hinge, the instability may occurs in the forward mode. Up to a certain velocity, the hub response after a disturbance follow a spiral motion that converge to the initial equilibrium point, but when the flutter speed is exceeded, so the stability limit is overstep, the response fall into a divergence spiral movement that bring the entire structure to fail (see right side of **Figure 1.3**).

Explain some fundamental aerodynamic property of pitching and yawing propeller, through reasoning on the blade element. Three possible motions are generate from whirl mode:

- angular displacement of the shaft in pitch ( or yaw);
- rate of change of pitch ( or yaw ) angle;
- lateral ( or vertical ) velocity of the shaft.

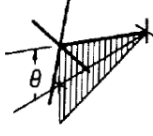
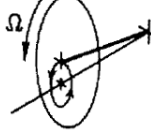
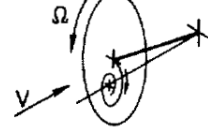
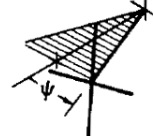
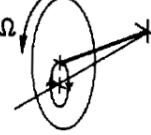
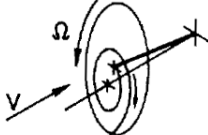
NATURAL VIBRATION MODES		
NONROTATING PROP.	ROTATING PROP. WITHOUT AIR FORCES	TRANSIENT RESPONSE WITH AIR FORCES
<p>PITCH</p> 	<p>FORWARD WHIRL</p> 	<p>STABLE (<math>V &lt; V_{CRIT}</math>)</p> 
<p>YAW</p> 	<p>BACKWARD WHIRL</p> 	<p>UNSTABLE (<math>V &gt; V_{CRIT}</math>)</p> 

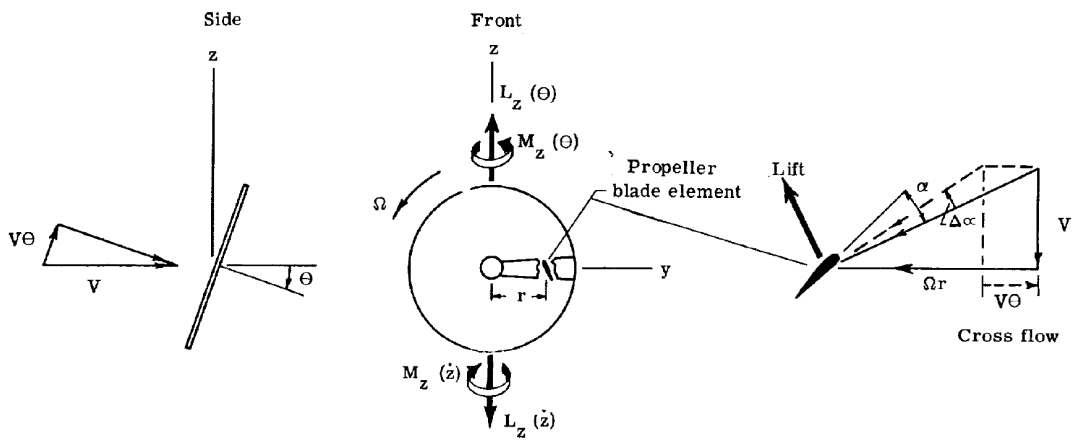
Figure 1.3: Natural vibration modes of system (from [12])

In the case where propeller shaft is inclined by a  $\theta$  angle, the forward velocity has a cross-flow component,  $V_\theta$ , in the plane of the propeller. Focusing on the blade element, it is noted that this cross-flow component decreases the AoA and the relative velocity in the up-going side of the propeller, instead opposite variations occur in the down-going side. Aerodynamic forces generated by these variations produces a vertical force  $L_z(\theta)$  and a yaw moment  $M_z(\theta)$ .

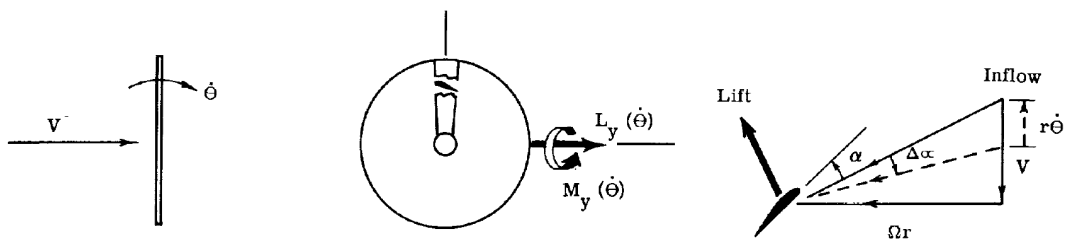
Yaw moment due to pitch,  $M_z(\theta)$  may be interpreted as a cross-stiffness term (**Figure 1.4a**). This moment is particularly important, because drive the system to the whirl flutter instability, it produce a moment in the same direction of the yawing velocity of the backward whirl mode. Moreover, this term acts as a negative aerodynamic damping, so to bring the system to stability is necessary to have other forces with positive damping. The force  $L_z(\dot{z})$  and moment  $M_y(\dot{\theta})$  produced respectively by  $\dot{z}$  and  $\dot{\theta}$  generate the aerodynamic damping required above. Moreover, during whirl the moment  $M_z(\dot{z})$  due by the vertical velocity, is in phase with the yaw angle, so it acts as an aerodynamic stiffness term. Similar consideration can also be made in the pitch rate case, as in **Figure 1.4b**. The inflow velocity  $r\dot{\theta}$ , due to the pitch rate produces an increase of the AoA in the disk area above the pitch axis and a reduction in the region below. Effects generate a damping moment  $M_y(\dot{\theta})$  and a cross-damping force  $L_y(\dot{\theta})$ . This cross-damping force behaves as a stiffness term in the yaw plane, in the same manner do the  $M_z(\dot{z})$ .

In conclusion, the important effect for the whirl flutter is the yaw moment due





(a) Pitch variation



(b) Pitch rate

Figure 1.4: Aerodynamic forces and moments on a pitching and plunging propeller at zero thrust (from [12])

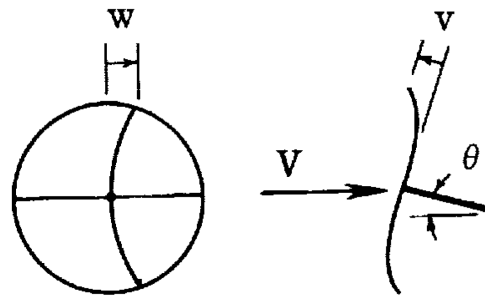


Figure 1.5: Rotor blade deformations due to the bending (from [12])

to pitch,  $M_z(\theta)$ , or the pitch moment due to yaw,  $M_y(\dot{\theta})$ . This cross-stiffness moment drives the system to the backward whirl mode and are counteracted by the aerodynamic and structural damping moments. Once the critical whirl flutter speed is reached, the energy input by the aerodynamic system exceeds the amount that can be neutralized by the damping, and the system drives to the fail of the structure.

In the tilt-rotor case, the presence of an articulated and flexible propeller-rotor system, a middle way between helicopter blade and aircraft propeller, alters the whirl flutter effects. Experimentally it has been seen, that the presence of a flapping blades increase the stability for backward whirl mode, but produces the opposite effects for the flutter in forward mode. Over the frequency changes, the rotor causes variations in the system behaviour, particularly in the forward whirl. Instead, unlike what was said above for the flapping motion, the bending motion of a twisted blade have components in the propeller plane but also normal to the plane, generating a bending vibration mode. The bending modes that can show a relationship with the whirl flutter are the cyclic pitch and cyclic flap motion, where the tip path plane is tilted by the bending deformation, **Figure 1.5** show this effects. Each of these modes are associated with a in plane component displacement, which are always lightly damped and potentially can be source of instabilities. So the blade flexibility has a relatively little effect for the stability of backward mode, except for the region where the ratio between bending frequency and the rotational velocity is close to the unity.

# Chapter 2

## Model description



Figure 2.1: Bell XV-15

For this work, the models used for the numerical simulations, are based on the Bell XV-15, shown in **Figure 2.1**, research aircraft with Advanced Technology Blades (ATBs) [7]. **Table 2.1** collects some generic information about this aircraft. A lot of investigations have been done on this model, so the good knowledge about stability derivatives makes this aircraft perfect for the analysis.

Based on the informations provided by [9, 1], a detailed CAMRAD/JA model has been built for the aeroelastic stability analysis. Dynamic model includes:

- airframe structural model;
- airframe stability and control derivatives;
- aeroelastic rotors;

Table 2.1: XV-15 Basic Information

Characteristic	Symbol	XV-15	Units
Gross Take-off weight	$W_{TO}$	13000	lb
Maximum engine(s) power	$P_{MAX}$	2 · 1550	hp
Maximum flight speed	$V_{MAX}$	280	kt
Wing span	$b$	32.17	ft
Wing area	$S$	169	$ft^2$
Rotor radius	$R$	12.50	ft
Rotor Solidity	$\sigma$	0.103	n.d.
Rotor Lock number	$\gamma$	3.768	n.d.
Rotor rotating speed	$\Omega$	601.0	rpm

- lumped parameter engine drive-train;
- rotor speed governor controller.

To follow the purpose of the work, an optimization process that involves both blade twist and the wing structure is needed, so the aircraft properties related to these parameter change every loop. This make necessary to analyse how the wing properties change with the variation of  $t/c$  ratio, because the wing normal modes and the aerodynamic derivatives are required as an input for the CAMRAD/JA analysis. This chapter is therefore divided in two sections, the first which explains how the modes are obtained when the thickness changes. The second section, on the other hand, deals with how the aerodynamic coefficients are estimated, always with variations in the thickness of the wing.

## 2.1 Normal Modes

As mentioned before, the natural frequency and the modes shapes are input data for the CAMRAD/JA analysis, but these properties are strictly related to the wing structure, so it is necessary to update the values every times the wing change thickness. The modes are computed with MSC NASTRAN analysis on a simplified finite-element model of the XV-15, reported in **Figure 2.2**. More details about the model are presented in the Appendix C of [1].

The use of this simplified model allows to simulate different wings thickness without change the model, modifying only the beam properties. So to compute the required data for the model, it is necessary to understand how the torsional and bending stiffness change as the wing  $t/c$  ratio changes. As was done in [1, 9, 11], the wing setup is different from the original aircraft: a graphite-epoxy conceptual wing is designed; reference values for the composite material are reported in **Table 2.2**.

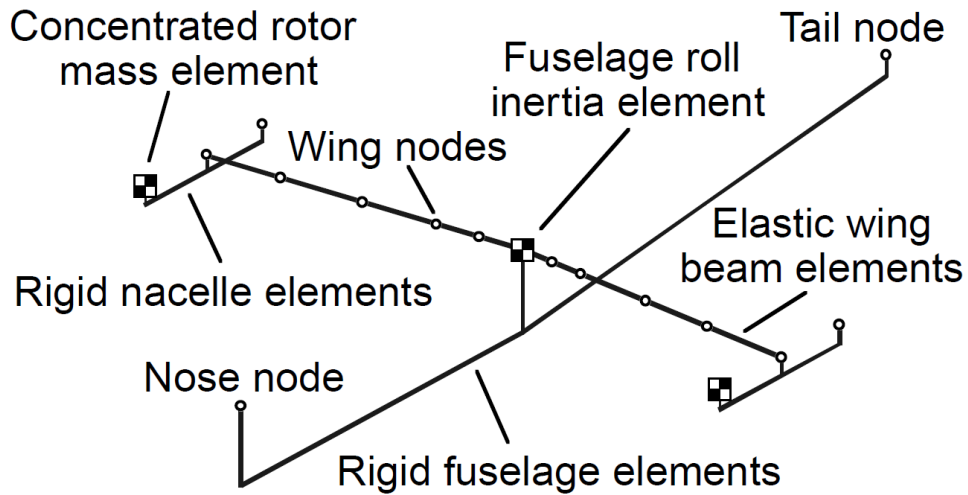


Figure 2.2: Nastran Finite-Element Model

Table 2.2: Graphite-epoxy material properties

Property	Value	Units
Elastic modulus, torque box	9000000	$\frac{lb}{in^2}$
Elastic modulus, spars	18000000	$\frac{lb}{in^2}$
Shear Modulus, torque box	3750000	$\frac{lb}{in^2}$
Density	0.06	$\frac{lb}{in^3}$
Limit strain	0.0047	$\frac{in}{in}$

Excluding the thickness, other geometric properties of the airfoil are not modified, therefore parametrizing the original profile, NACA64A223, with respect to the aerodynamic chord and then scaling these coordinates with the  $t/c$  ratio, allows to obtain all the airfoils shapes. Once the section shape is defined, using the semi-monocoque approach is possible to compute the stiffness properties. As made in [1], a single torque box model, **Figure 2.3**, with six stringers and two web, is used for analysis.

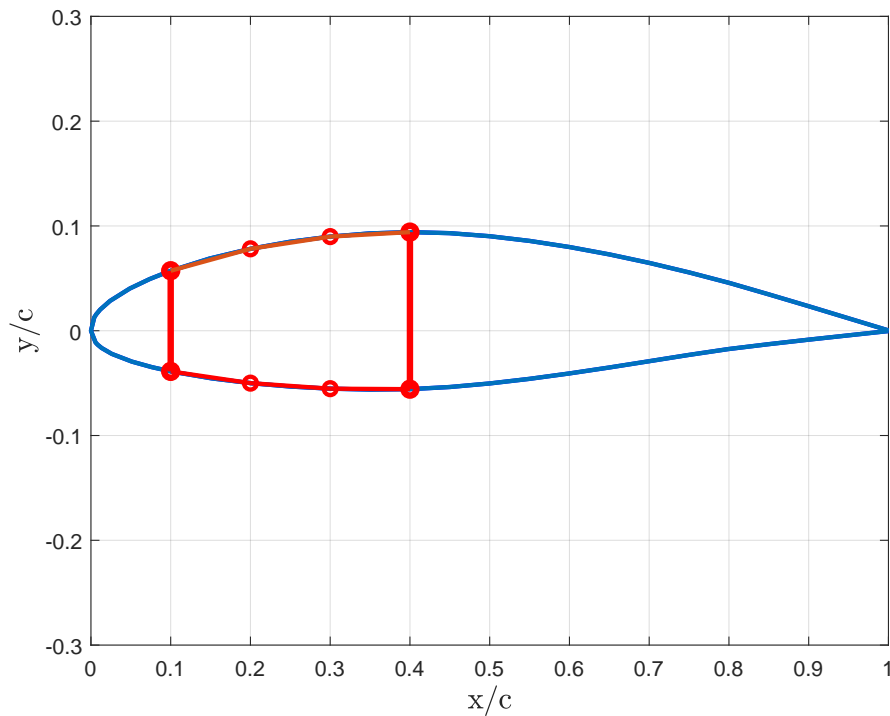


Figure 2.3: Single cell torque box

The first thing is to compute the section properties as function of the panel and web thickness. An inverse design approach is adopted to find a reasonable value based on the stiffness values provided by [1] for the section with  $t/c = 0.15$  presented in **Table 2.3**.

Table 2.3: Wing properties from Acree's reference

Characteristic	Value
$t/c$	0.15
Beam bending	1.98e+09
Chord bending	7.59e+09
Torsion	1.33e+09

Create a system with two equations, torsional and bending stiffness, considering the skin contribution as the 15% of total bending stiffness value. In this system the only unknowns are the web and panels thickness, so it can be solved in close form. Once the two optimal value are available, it is possible to create the torque box for each section. Using the semi-monocoque approach with the same torque box structure for different airfoil thickness, and compute for each of it  $K_\theta$  value, is possible to interpolate the results to obtain a generic law for the torsional stiffness. **Figure 2.4** shows the obtained law.

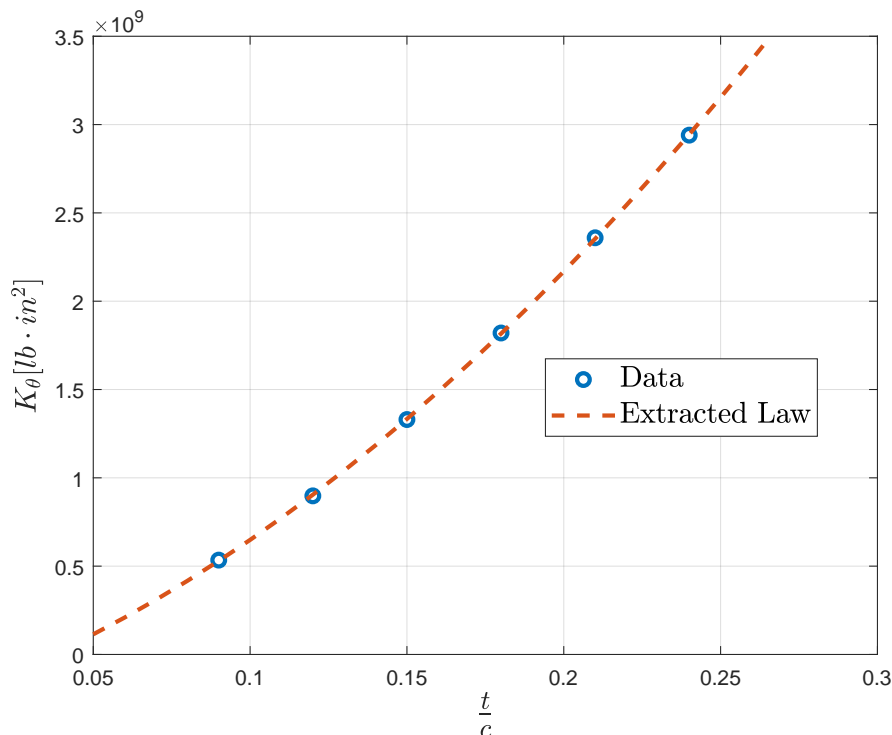


Figure 2.4: Torsional stiffness trend respect thickness

Once the torsional stiffness as function of the  $t/c$  ratio has been obtained, it is possible to update the finite element model, knowing only the  $t/c$  ratio, and then perform the MSC NASTRAN analysis to evaluate the frequencies and modes shape. From the MSC NASTRAN output file extract the frequency and the displacement of first six mode, symmetric and antisymmetric wing bending (SWB/AWB), symmetric/antisymmetric wing chord (SWC/AWC), and symmetric/antisymmetric wing torsion (SWT/SWT), which will then be used as input in the CAMRAD/JA model. Following the indication of [9], a 1.5% of structural damping has been considered for each mode.

## 2.2 Aerodynamics

CAMRAD/JA input file requires also the coefficients for aerodynamic derivatives, also in this case the parameters need to be updated before the CAMRAD/JA analysis with respect to the wing thickness during the optimization. To do that, the selected approach is to built a database, which contains the aerodynamic coefficients for different wing thickness, evaluated for several AoA and forward velocity. The program used to built the database is XFRL5, software for the 3D aerodynamic analysis, based on Xfoil. With this program it is possible to design a 3D wing model, and evaluate the aerodynamic coefficients selecting the desired condition for the simulation. **Table 2.4** shows real data of the XV-15 used to built the 3D wing [7]; the resulting model is shown in **Figure 2.5**. The wing planform is the same for each model, but the one that changes is the main wing airfoil, which varies with the  $t/c$  ratio.

Table 2.4: Aerodynamic Surface Data from real XV-15

Wing	Symbol	Value	Unit
Span	b	32.17	ft
Area	S	169	$ft^2$
Chord	c	5.25	ft
Sweep	$\Lambda$	-6.5	$deg$
Dihedral	$\Gamma$	2	$deg$
Aspect Ratio	$AR$	6.12	n.d.
<b>Horizontal tail</b>			
Airfoil	NACA 64A015		
Span	b	12.83	ft
Area	S	50.25	$ft^2$
Chord	c	3.92	ft
Aspect Ratio	$AR$	3.27	n.d.
<b>Vertical Tail</b>			
Airfoil	NACA 0009		
Area	S	50.5	$ft^2$
Chord	c	3.72	ft
Aspect Ratio	$AR$	2.33	n.d.

To verify how realistic the values produced by XRFL5 are, real wind tunnel results provided by Ferguson [5] are used for the comparison. The simulations for low speed values does not produce any problem, but increasing the speed value the simulations showed some problems of convergence for several AoA, due to high Reynolds number ( $Re$ ). So to obtain the aerodynamic coefficients for higher



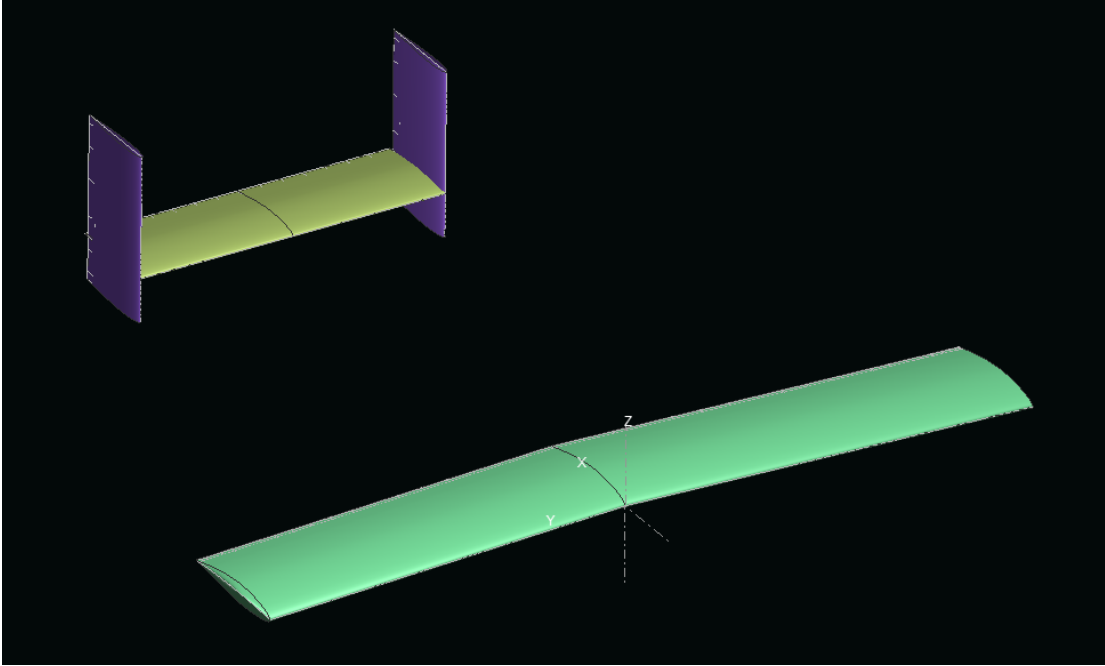


Figure 2.5: XV-15 Model for the Aerodynamic Analysis in XFRL5

speed values, Mach correction shown in **Equation (2.1)** is used on low speed coefficients. This is reasonable because using the same correction on the real low speed data provided by Ferguson, the results at higher velocity are very close to the experimental data at the same speed, see for example **Figure 2.6**.

$$C_{LMHigh} = \frac{C_{LMLow}}{\sqrt{1 - M^2}} \quad (2.1)$$

For the drag ( $C_D$ ), to match the real value, it is necessary to take into account the resistance due to the nacelle. So to do that, an extra drag is added in each analysis, based on the zero lift drag coefficients provided by Ferguson for the wing pylon, see **Equation (2.2)**.

$$S_{WP} \cdot C_{DFerg} = S_W \cdot C_{DW} + S_{extra} \cdot C_{Dextra} \quad (2.2)$$

$$\left\{ \begin{array}{ll} S_{WP} = 181 ft^2 & \text{Wing Pylon Surface} \\ S_W = 169 ft^2 & \text{Wing Surface} \\ S_{extra} = 181 - 169 = 12 ft^2 & \text{Nacelle Surface} \\ C_{DFerg} = 0.01777 & \text{Real Value} \\ C_{DW} = 7.52 \cdot 10^{-3} & \text{Only Wing - Xfrl5} \\ C_{Dextra} & \text{Nacelle Drag} \end{array} \right.$$

For high speed analysis is necessary to update the extra drag value, otherwise Mach correction only is not enough to match the real high speed drag coefficients.

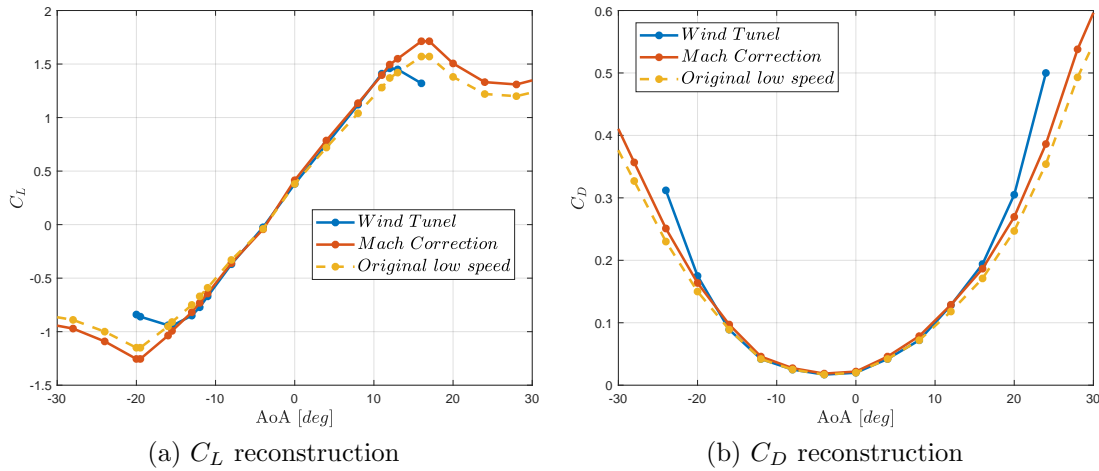


Figure 2.6: Wind tunnel values for  $M = 0.4$  compared with the aerodynamic coefficients at the same speed reconstructed from low speed wind tunnel values

This means that for the reason mentioned before, the analysis converges only for low AoA, but this is enough for a whirl flutter investigation. In conclusion, to obtain the aerodynamic coefficients, for each wing model, two different analysis are made, one at low mach number ( $M \approx 0.1 - 0.2$ ) to obtain the basic values that can be update using the mach correction for higher speed values, and one at high mach number ( $M \approx 0.6$ ) to update the value for the drag coefficient, all the parameters used in XFRL5 for the analysis are listed in details in **Table 2.5**. See **Figures 2.7, 2.8, 2.9** for the aerodynamic results, for different mach velocities.

Table 2.5: Parameters for XFRL5 analysis

Parameter	First Analysis	Second Analysis
Velocity	76 mph	455 mph
Analysis Type	3D	3D
Ref. Dimensions	Wing Planform	Wing Planform
Extra Drag	Area = 12 ft <sup>2</sup> $C_{D_0} = 0.161$	Area = 12 ft <sup>2</sup> $C_{D_0} = 0.5049$

**Figure 2.10** therefore shows how the aerodynamic coefficients are influenced by the thickness value, for clarity of reading only some values have been reported so as to be able to better appreciate the changes in the trend. As can be seen from the plots, the  $C_L$  value increases with the thickness, thus generating more lift, also necessary to support the greater weight due to the increase in the size of the wing. Similar discourse for resistance, where however the difference between the resistance coefficients becomes more visible as the AoA increases.

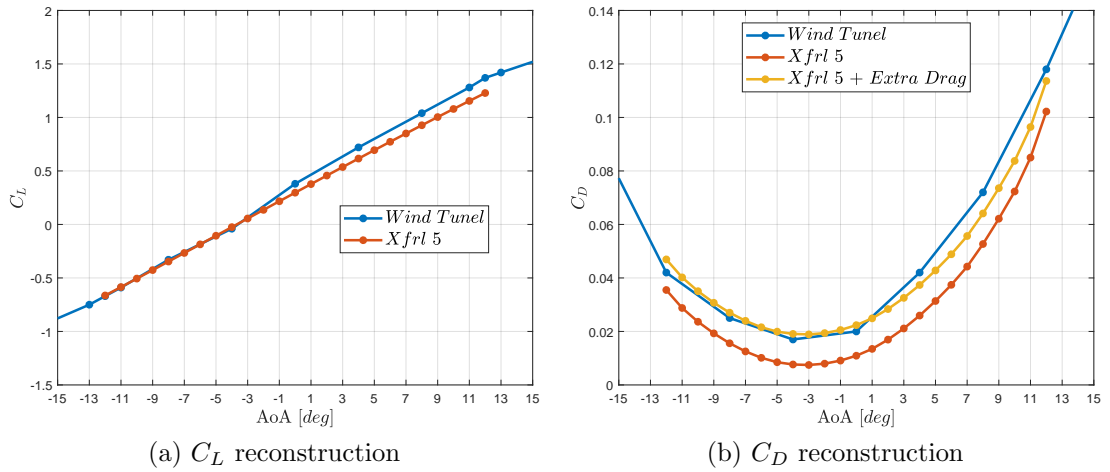


Figure 2.7: Aerodynamic coefficients for  $M = 0.1$  from Xfrl5 respect real values

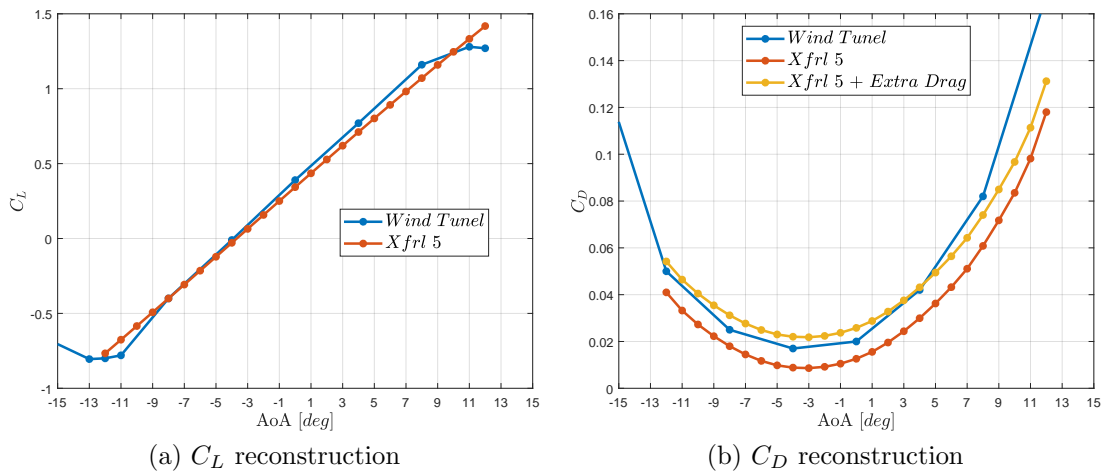


Figure 2.8: Aerodynamic coefficients for  $M = 0.5$  from Xfrl5 respect real values

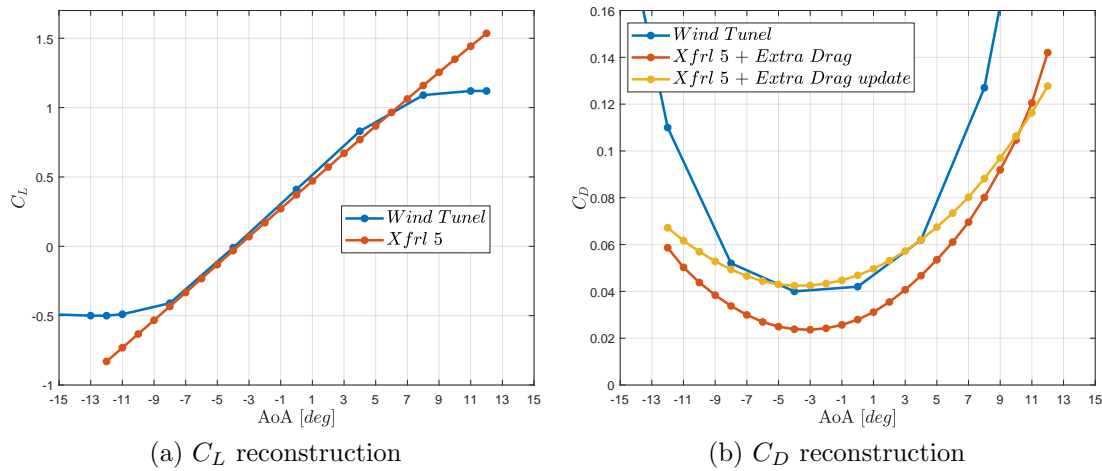
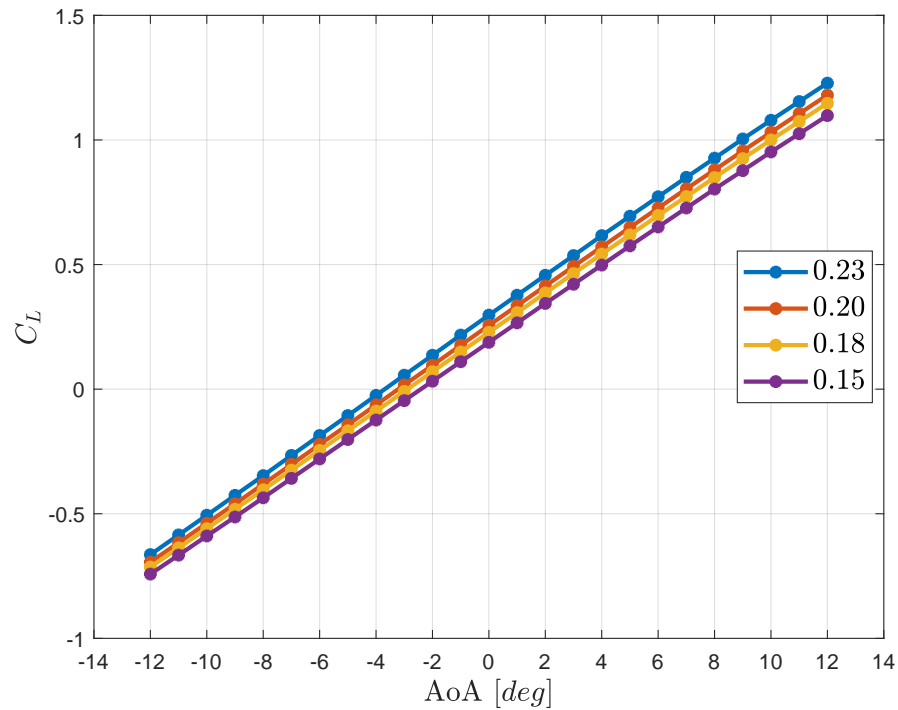
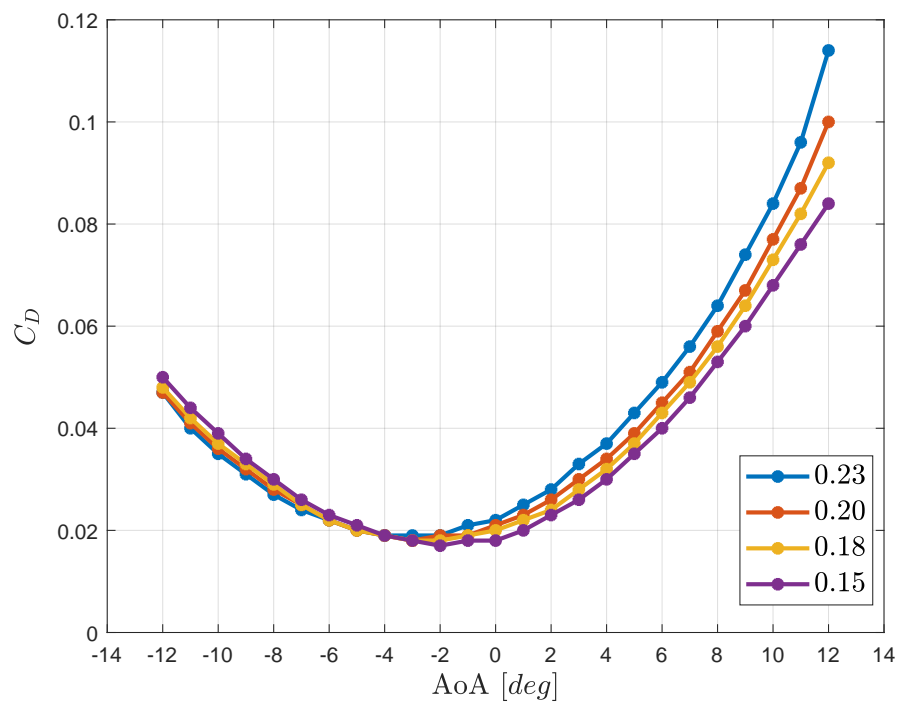


Figure 2.9: Aerodynamic coefficients for  $M = 0.6$  from Xfrl5 respect real values

Once the database is built for the different airfoil thickness, the last step is to use the respective data to compute the aerodynamic derivatives required for the CAMRAD/JA input file. During the optimization, based on the current value of the  $t/c$  ratio, aerodynamic coefficients are extracted from the database, then the total lift, drag and moment are computed, considering the fuselage contribution (fuselage data available on [5]), and finally the curves are interpolated and derived by the respective parameter required by CAMRAD/JA. Then the values computed for the derivatives are reported in the CAMRAD/JA input file and updated for each velocity analysed in the simulation.

(a)  $C_L$ (b)  $C_D$ Figure 2.10: Behaviour of aerodynamic coefficients for different thickness values -  $M = 0.2$



# Chapter 3

## Optimization scheme

The chapter describe the optimisation procedure used in order to find the best solution in terms of whirl flutter velocity. The first section, briefly describe the selected algorithm, and the reasons why it was chosen. The second section show the problem formulation and explain the optimization procedure.

### 3.1 Optimization Algorithm

The problem to be analyzed consists in going to look for a combination of variables that will minimize a particular objective function, which in our case is represented by the desire to maximize the whirl flutter speed, while respecting the constraint imposed on the maximum power value. To do this constrained minimization problem, the Matlab function *fmincon* is selected. It allows to find the minimum of constrained non-linear multi variable function, with the possibility of changing the algorithm used according to the nature of the problem. The selected algorithm from the *fmincon* set, is the *Interior Point Algorithm*, that solves the original constrained minimization problem, solving a sequence of approximate problems. The original problem is:

$$\min_x f(x), \text{ subject to } h(x) = 0 \text{ and } g(x) \leq 0 \quad (3.1)$$

where  $f(x)$  represents the function whose minimum is desired,  $x$  the vector of the available variables, and  $h(x)$  and  $g(x)$ , respectively the linear and non-linear constraints. And for each  $\mu > 0$ , the approximate problem is:

$$\begin{aligned} \forall \mu > 0 \quad \min_{x,s} f_\mu(x, s) &= \min_x f(x) - \mu \sum_i \ln(s_i) \\ &\text{subject to } h(x) = 0 \text{ and } g(x) + s = 0 \end{aligned} \quad (3.2)$$

where  $s_i$  is the slack variable for the  $g_i$  constraints, and must be positive to keep  $\ln(s_i)$  bounded. As  $\mu$  decreases to zero, the minimum of  $f_\mu$  should approach

the minimum of  $f$ . The added logarithmic term is called a barrier function. Among the possible algorithms proposed by the *fmincon*, the choice to use the *interior point algorithm* depends on the fact that it is able to handle large, sparse problems, as well as small dense problems. The algorithm satisfies bounds at all iterations, and can recover from not a number (NaN) or infinite results. Moreover, it is one of the fastest to converge among those proposed by Matlab, an important characteristic, as it allows to arrive at a solution with fewer iterations, limiting the number of analyses in CAMRAD/JA that require a lot of time to carry out. More details about the step selection and problem solution are reported in the Matlab documentation [6].

## 3.2 Optimization structure

The aim of the optimization process is to maximize the whirl flutter velocity, under the maximum power constraint. Velocity and power are expressed respect the respective baseline value, in order to work with small and comparable values. The power value is computed always at the dive speed velocity, in order to obtain the power in the same condition for each obtained configurations. The resulting constrained minimization problem is:

$$\min_x f(x) = \frac{V_{wfo}}{V_{wf}} \quad (3.3)$$

$$\min_x f(x) = \begin{cases} c(x) < 0 \rightarrow c(x) = \frac{P}{P_0} - 1 \\ \text{lb} < x < \text{ub} \end{cases} \quad (3.4)$$

where  $x$ , is the optimization variable vector, which is composed by a series of linear slope for the blade twist, based on the number of blade sections, the radial positions where the slope changes, and finally the  $t/c$  value. Lb and ub are respectively, the upper bound and lower bound vectors, which contain the limit values for the range of variation of the vector  $x$ .

To evaluate the objective function is necessary for each iteration to compute the whirl flutter velocity and aircraft power required with respect to the current value of  $x$ . So, the process starts with the evaluation of wing modes through MSC NASTRAN analysis and the extrapolation of aerodynamics coefficients from the database, next the CAMRAD/JA input file is built for this specific combination of slopes and  $t/c$  ratio, then after a post-processing on the CAMRAD/JA results, the values for whirl flutter velocity and power are extrapolated, and then once the constraint on power is evaluate, the function compute a new state and the process restarts until the program find a minimum for the function. The block diagram in **Figure 3.1** summarizes the optimization process.



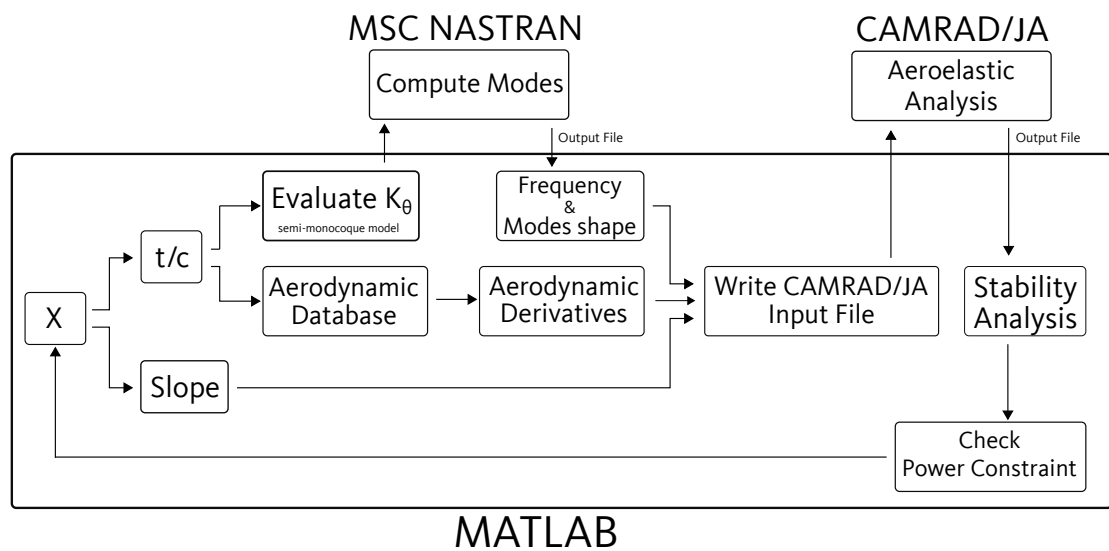


Figure 3.1: Optimization procedure scheme



# Chapter 4

## Rotor twist optimization

In this chapter the results obtained from the optimization process are presented and discussed. The chapter is divided into several sections, the first section shows what is the reference condition used for optimization. The second section shows overall the results obtained, then going to investigate in detail the global minimum found for each approach used. The third and fourth sections, on the other hand, always deal with the optimal solutions seen in the previous section, but analyzed in different trim conditions, respectively with maximum fixed power and in helicopter mode.

### 4.1 Reference Case

The reference configuration used in the optimization procedure, is the basic solution used by Acree [1], because the real XV-15 wing is very stiff due to the high thick to chord ratio ( $t/c = 0.23$ ) and whirl-mode instability does not occur inside the range of examined velocities. Furthermore the low thickness of this solution allows to see the effects introduced by any variation on the wing thickness and on the blade twist. Rotor geometry follows the real XV-15 values, the blade twist law used in the reference case is a linear regression based on the real XV-15 blade twist distribution. **Figure 4.1** shows comparison between the two blade twist laws.

CAMRAD/JA stability analysis on this reference configuration are performed to obtain the baseline values for the optimization process. **Figures 4.2 4.3** show respectively the trend of symmetric and antisymmetric parts of whirl-modes respect the forward flight velocity. From the results, critical modes are SWC and AWB respectively, which exactly reflect what Acree predicted [2]. **Table 4.1** summarizes all the parameters of the reference solution, whirl flutter velocity and power computed at dive speed. Values found here will be those used to evaluate the objective function and the power constraint during the optimization procedure.

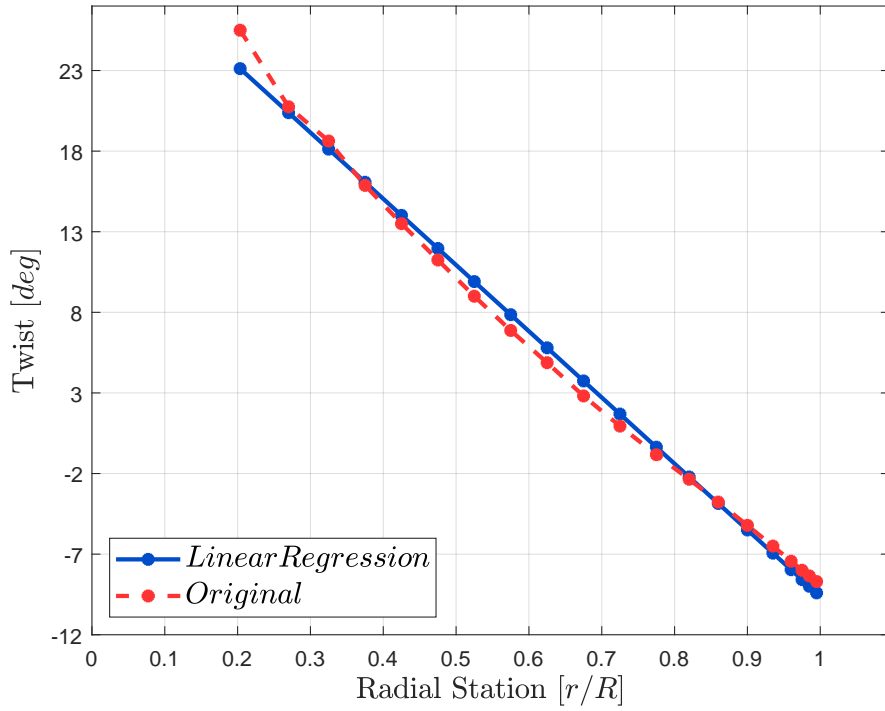


Figure 4.1: Linear regression and real blade twist distribution

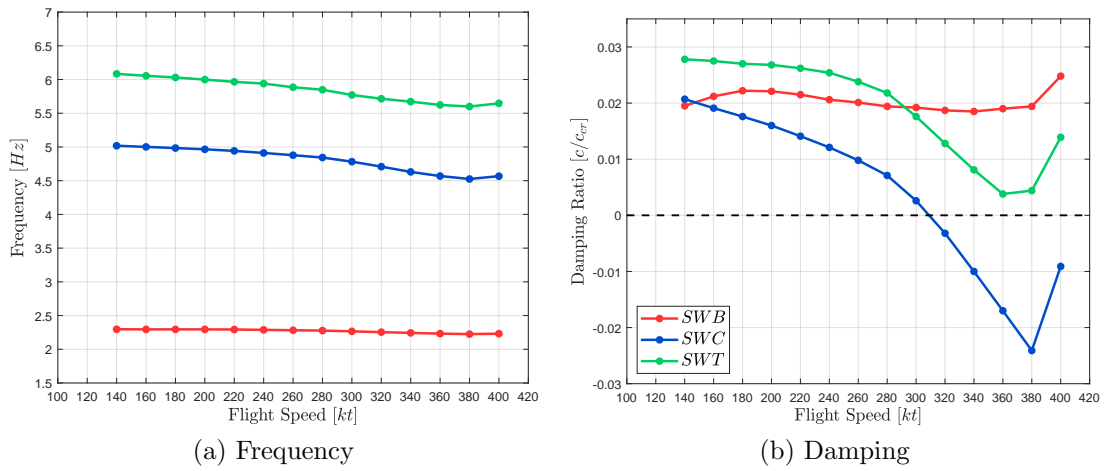


Figure 4.2: Whirl-mode frequency and damping w.r.t. flight speed - Symmetric roots

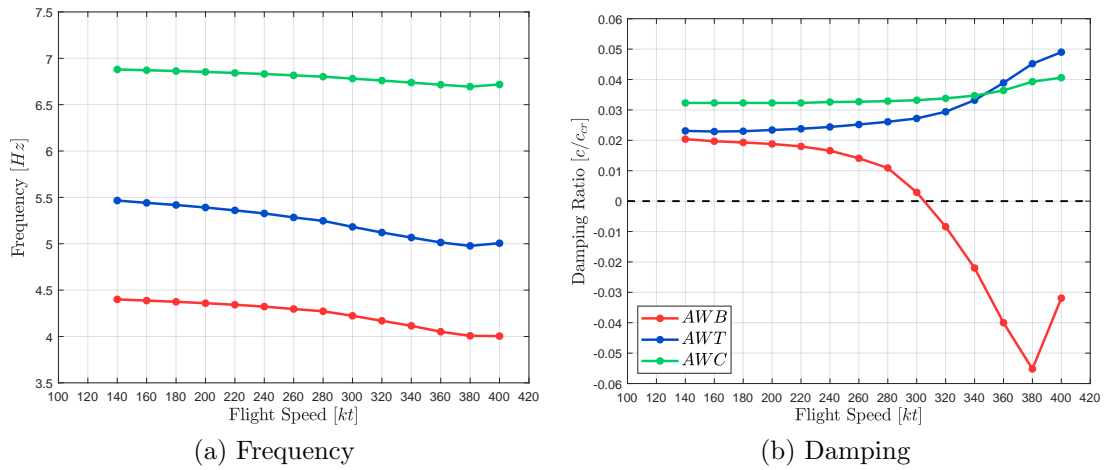


Figure 4.3: Whirl-mode frequency and damping w.r.t. flight speed - Antisymmetric roots

Table 4.1: Reference Solution

Characteristics	Symbols	Values	Units
Thick to chord ratio	$t/c$	0.15	—
Twist slope	$\theta_{tw_0}$	-41.086	$\frac{deg}{r/R}$
Whirl flutter velocity	$V_{wfo}$	305.23	$kt$
Dive velocity	$V_m = \frac{V_{wfo}}{1.15}$	265,41	$kt$
Required power	$P_0(V_m)$	944,89	$Hp$

## 4.2 Optimization Procedure

Several analysis have been performed using different starting points and changing the structure of the optimization variable vector:

- first approach is to leave free to change the blade twist slope and the  $t/c$  ratio;
- second approach is to divide the blade into two segments, each with its slope, thus obtaining a piecewise linear twisting law. The radial station in which the slope change takes place is also a parameter of the optimization, that can change between the blade cutout ( $r_0/R = 20\%$ ) and the blade tip;
- third approach follow the second routine, but this times the blade is divided into three different segments so the variable vector is composed by three slopes, two radial positions for the slope change and the thick to chord ratio value.

All the twist law have been defined independently from the slope values to obtain zero twist at the 75% of blade span with null collective pitch. The effects of blade twist variation have been introduced and discussed previously in the introduction , and are widely discussed in Ref [9]. Generally, decreasing slope increase the whirl flutter stability due to the positive pitch-lag coupling effects generated by the positive trim angle, that is a consequence of the shifting of the total thrust toward the blade tip. Decreasing slope also increases the required power due to the higher induced drag generated by the high lift at the tip section. Opposite consideration in the case of increasing slope, decrease the whirl flutter stability with a limited decrease of required power. All the analyses are performed considering the same trim condition, level flight with unlimited power. Obviously this is an unrealistic condition, but allows to compute the whirl flutter velocity and the relative required power, in order to compare the different solutions. The rotor is trimmed to 480.8 rpm (80% of hover design rpm) at Sea Level Standard (SLS) ISA + 0°C flight conditions.

## 4.3 Optimization Results

All the optimization results are summarized in the **Table 4.2**. Each case shown in the table represents a different optimization, obtained starting from a different initial guess. Each solution obtained represents a possible local minimum for the objective function, divided according to the number of segments into which the blade was divided.

From the optimization results it is easy to identify the trend of each solution to increase the wing thickness. This generate a stabilizing effect from the whirl flutter

Table 4.2: Optimization Results

Case	Slopes	$\theta_{tw_1}/\theta_{tw_0}$	$\theta_{tw_2}/\theta_{tw_0}$	$\theta_{tw_3}/\theta_{tw_0}$	$r_1/R$	$r_2/R$	$t/c$	$V_{wf}$ [kt]	$f$ $V_{w,f_0}/V_{wf}$	Increase [%]	$P(V_m)$ [Hp]	$P/P_0$ [%]
1	1	1,0300	-	-	-	-	0,160	336,88	0,906	10,37%	937,32	0,992
2	1	1,0220	-	-	-	-	0,172	350,83	0,870	14,94%	943,25	0,998
3	1	1,0250	-	-	-	-	0,174	355,22	0,859	16,38%	940,97	0,996
4	1	1,0268	-	-	-	-	0,172	350,61	0,871	14,87%	939,65	0,994
5	2	1,0393	-	-	-	-	0,167	339,55	0,899	11,24%	930,71	0,985
6	2	1,1000	0,9000	-	60%	-	0,160	327,17	0,933	7,19 %	938,36	0,993
7	2	1,2229	0,8502	-	60%	-	0,173	352,50	0,866	15,49%	889,40	0,941
8	2	1,1382	1,0363	-	40%	-	0,174	354,63	0,861	16,19%	908,62	0,962
9	2	1,2306	1,0949	-	53%	-	0,175	357,85	0,853	17,24%	891,21	0,943
10	2	1,2239	0,8453	-	60%	-	0,172	352,14	0,867	15,37%	889,61	0,941
11	2	1,2242	0,7370	-	60%	-	0,171	355,44	0,859	16,45%	905,86	0,959
12	2	1,2000	0,7500	-	62%	-	0,160	325,05	0,939	6,50 %	906,23	0,959
13	2	1,2131	0,9699	-	45%	-	0,175	356,52	0,856	16,81%	903,21	0,956
14	2	1,3000	0,7000	-	55%	-	0,160	330,26	0,924	8,20 %	917,06	0,971
15	2	1,1000	0,8500	-	70%	-	0,170	355,52	0,859	16,48%	917,28	0,971
16	2	1,2500	0,7000	-	52%	-	0,174	359,78	0,848	17,87%	930,13	0,984
17	2	1,2320	0,7200	-	62%	-	0,173	358,52	0,851	17,46%	893,48	0,946
18	2	1,1500	0,7500	-	70%	-	0,170	355,08	0,860	16,33%	903,89	0,957
19	3	1,2390	0,9292	0,7768	41%	64%	0,165	353,76	0,863	15,90%	936,64	0,991
20	3	1,2965	0,8866	0,8058	42%	57%	0,171	354,53	0,861	16,15%	927,27	0,981
21	3	1,1748	0,9711	0,926	40%	48%	0,173	361,74	0,844	18,52%	944,44	1,000
22	3	1,3120	0,9147	0,7954	42%	62%	0,172	352,29	0,866	15,42%	913,72	0,967
23	3	1,2868	1,0234	0,9648	45%	76%	0,174	356,52	0,856	16,81%	885,29	0,937
24	3	1,3500	0,9200	0,78	40%	65%	0,172	353,00	0,865	15,65%	927,04	0,981

point of view, due to the fact that torsional stiffness of the wing is directly connect to the whirl-mode instability, higher torsional stiffness increases the stability limit of whirl flutter. **Figure 4.4** shows the effects of thickness variation on the whirl modes damping, changing the  $t/c$  from 0.15 to 0.17, approximately the value where all the optimization solutions converge.

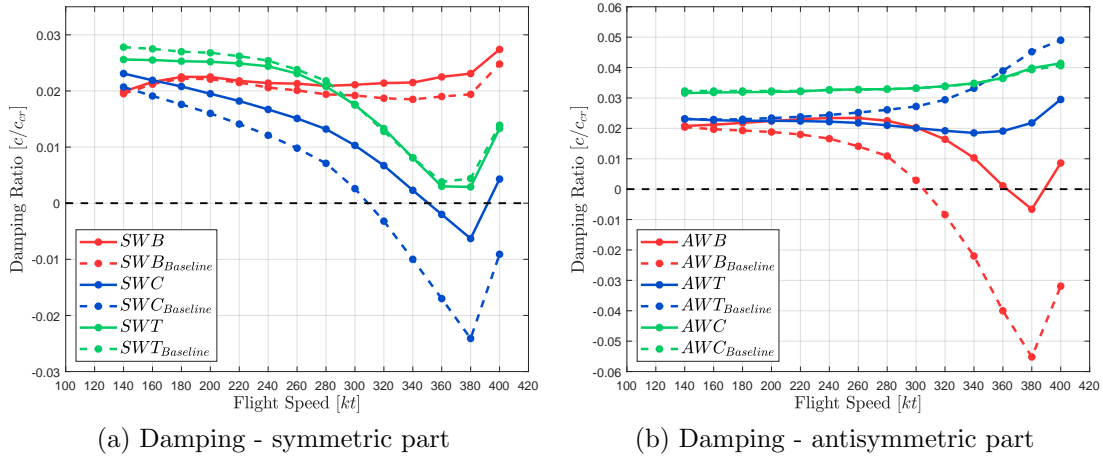


Figure 4.4: Whirl modes damping variation changing the  $t/c$

From the results it is evident that the two more critical modes, the SWC and AWB increase their stability limit, reaching a whirl flutter velocity up to 350, 7 kt. The variations mainly influence this two modes, but it is also interesting to note how the AWT damping decreases with the velocity, while the SWT remains almost unchanged. At the same time, the increase of thickness modify the aerodynamic performance of the wing, increasing the drag, that generates in turn an increase in the required power. In fact respect the baseline, the configuration with only thickness increase ( $t/c = 0.17$ ) at the dive speed require  $P(V_m) = 960,95$  Hp. So to satisfy the power constraint, the slope of twist distribution must increase, in order to find a trade off between its destabilizing effect in the whirl-mode and the consecutive reduction in the total required power. This behaviour is particular evident in the one slope case, where the number of variables for the optimization is reduced, so the solutions move toward the stabilizing effects due to the higher stiffness sacrificing the aerodynamic efficiency. For the solutions with multiple segments available, results show the tendency to increase the slope value in the blade root and then decrease it near the blade tip. This means, that in the searching of a possible trade off between the stability limit and the aerodynamic performance, at blade root, twist slope can increase significantly, in order to recover the increase of power required by the higher thickness, at the blade tip instead, where the aerodynamic performances are more important, the twist slope decreases, recovering part of the stability and improving the rotor performance. Possibility of optimizing several variables, including the same position where the change of



slope takes place, is reflected in the obtained results. In fact the slope values in the multi-segment optimization shows higher variations than the previous solutions, thus allowing to increase their effects on stability and aerodynamic performance. Among the possible local minimums found, for each approach, there is an optimal solution that provides the maximum increase in the whirl flutter speed, which represents the global minimum of the object function.

### 4.3.1 Single slope case

For this approach the number of optimal solutions found is low, because a lot of them does not converge or points toward a set of very close values. In fact, many solutions found have not been reported, because they had minimal differences in the values of the variables, reflecting in practically identical whirl flutter speed and power values. The best solution found is the case number three, which shows a whirl flutter velocity increased by 16.38% with respect to the baseline, while keeping at the same time the power required equal to 99.59% of the maximum available power, details are summarize in **Table 4.3**. **Figure 4.5**, shows the twist distribution with respect to baseline case, the two solutions are very close especially in the blade root but the stability limit is very different, showing of how much torsional stiffness affects the whirl flutter.

Table 4.3: Sol 3 - results summary

Characteristics	Symbols	Values	Units
Thick to chord ratio	$t/c$	0.174	–
Twist slope ratio	$\theta_{tw_1}/\theta_{tw_0}$	1.025	–
Whirl flutter velocity	$V_{wf}$	355.22	$kt$
Power	$P(V_m)$	940,97	$Hp$

Despite the increase of torsional stiffness, the two critical whirl-mode remain the SWC and AWB, though only the SWC becomes unstable, AWB damping comes close to the stability limit, but without going beyond it. All whirl-mode damping and frequency of the solution three are shown in **Figures 4.6 4.7**. More or less, for each mode the frequency increases, especially for chord and torsion modes. So increasing the blade twist by the 2.5%, allows to reduce the required power, without penalizing more the stability provided by the thickness increase.

### 4.3.2 Two slope case

Optimization with the blade divided into two segments generates many different solutions, but among these, the one that produces the best results is number 16.

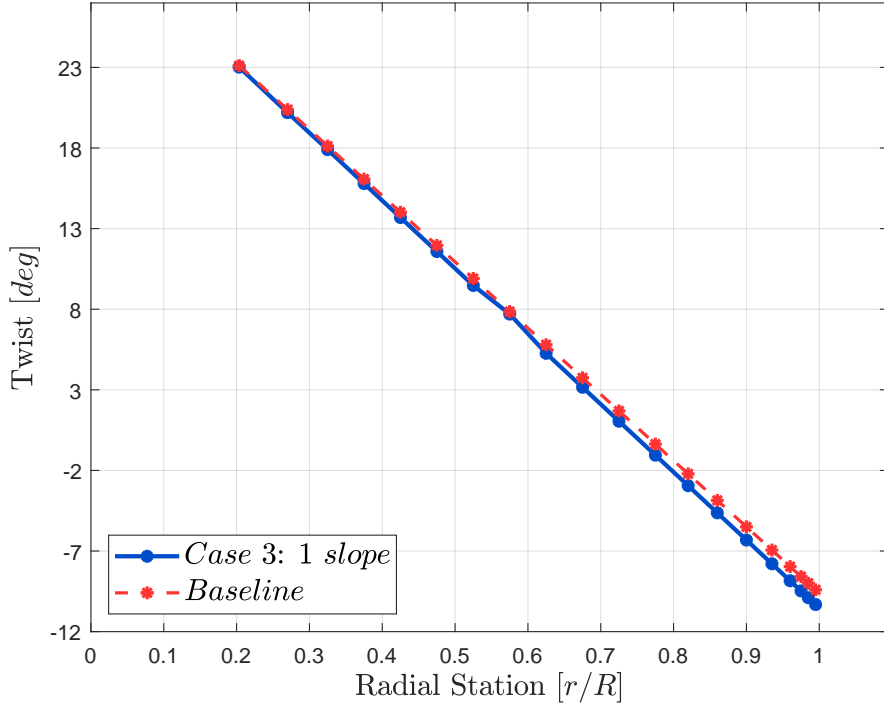


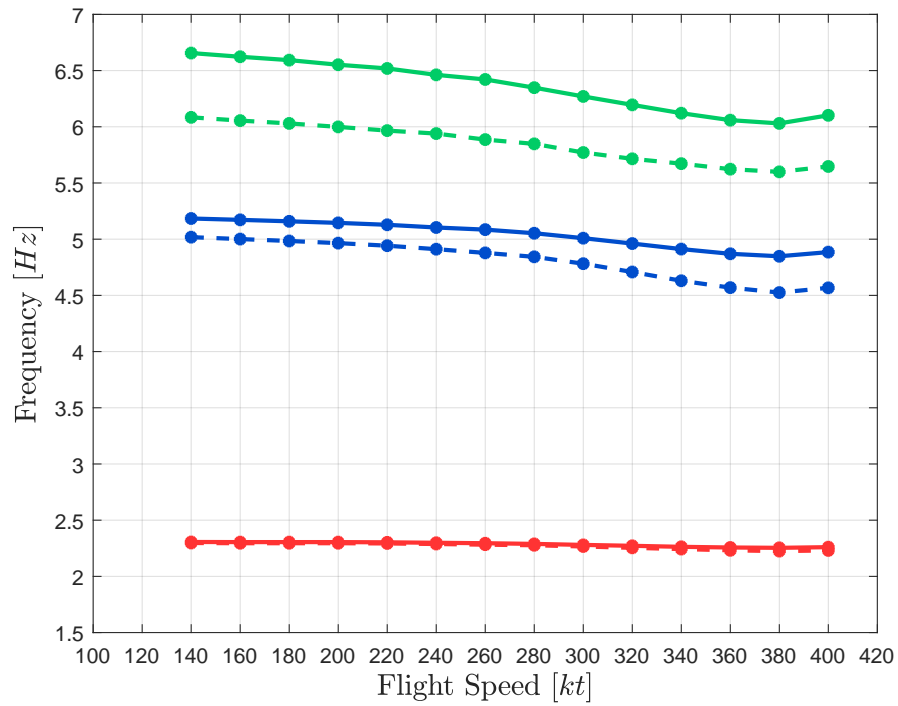
Figure 4.5: Solution 3 - Twist distribution

Twist distribution of this solution, shown in **Figure 4.8**, presents a larger increase of slope in the first part of the blade, joined with a rapid decrease near the tip. This configuration increases the whirl flutter velocity by 17,87%, using only the 98,44% of maximum available power, all the other details of the solution are reported in **Table 4.4**.

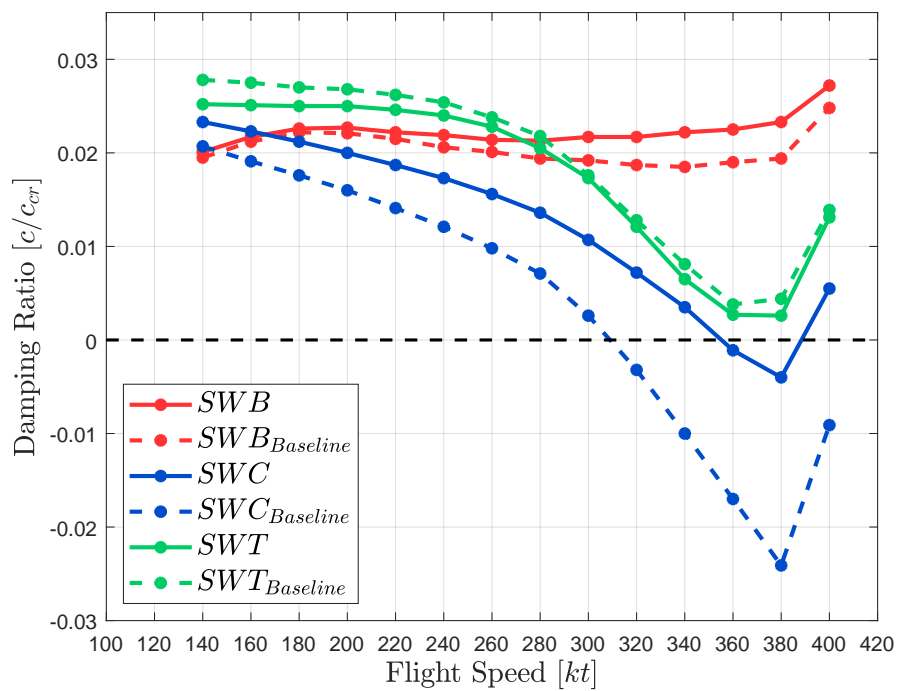
Table 4.4: Sol 16 - results summary

Characteristics	Symbols	Values	Units
Thick to chord ratio	$t/c$	0.1735	—
Twist slope ratio - First segment	$\theta_{tw_1}/\theta_{tw_0}$	1.25	—
Twist slope ratio - Second segment	$\theta_{tw_2}/\theta_{tw_0}$	0.7	—
Slope change radial station	$[r/R]$	52%	—
Whirl flutter velocity	$V_{wf}$	359.78	$kt$
Power	$P(V_m)$	930,13	$Hp$

In **Figures 4.9 4.10** are reported the trend of whirl-mode extrapolated from CAMRAD/JA. Critical modes in the symmetric part are the SWT and SWC, but in this case the critical velocity is given by SWT. Instead for antisymmetric part the instability comes in the AWB as expected. Respect to the baseline solution, and the previous consideration made on the thickness variations, the higher



(a) Frequency



(b) Damping

Figure 4.6: Solution 3: Whirl-mode frequency and damping w.r.t. flight speed - Symmetric roots

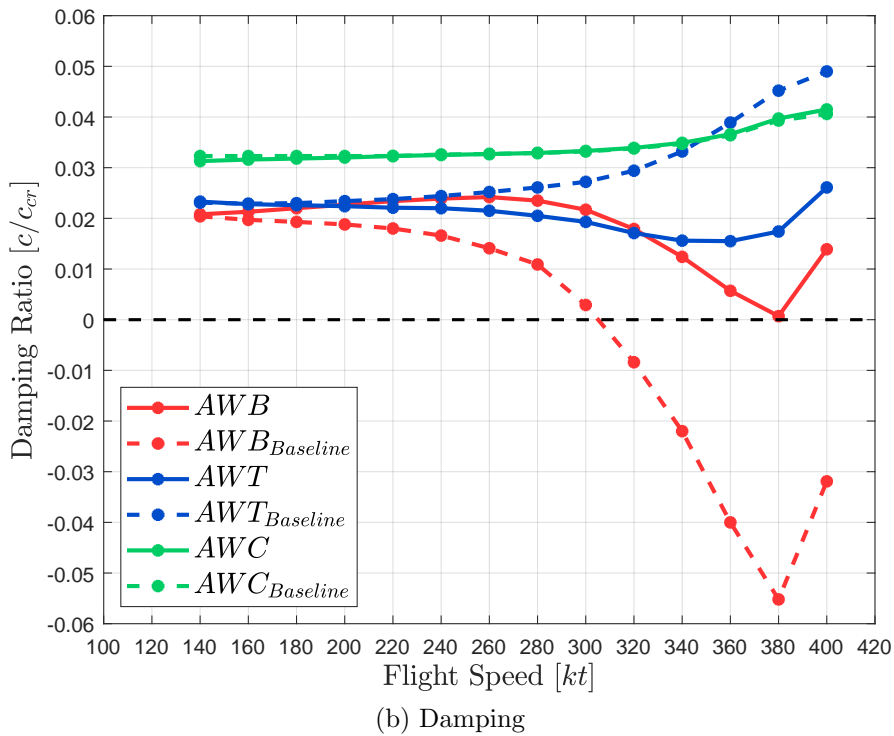
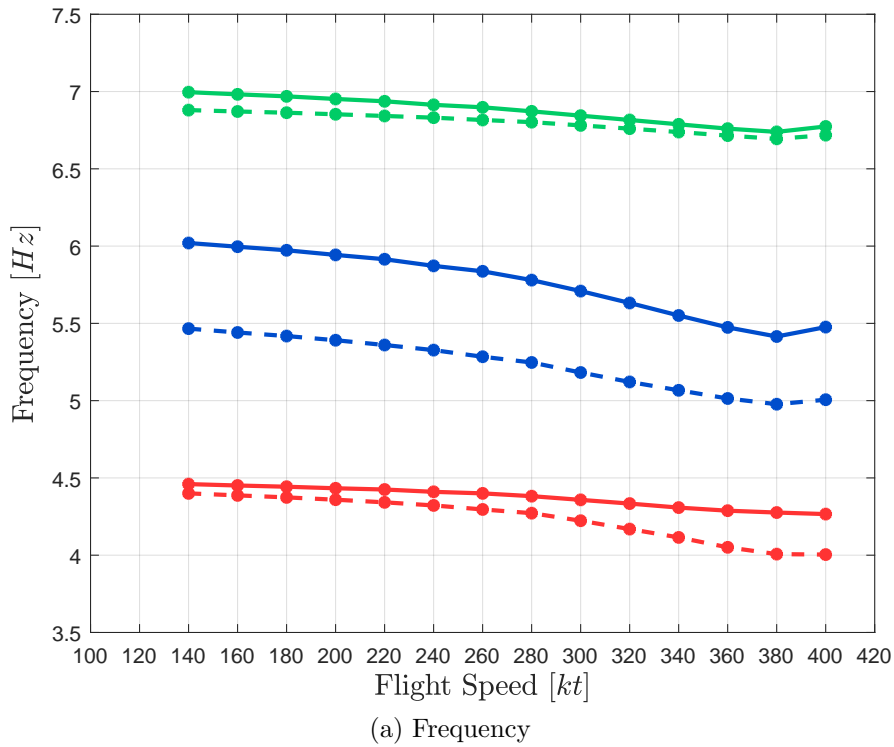


Figure 4.7: Solution 3: Whirl-mode frequency and damping w.r.t. flight speed - Antisymmetric roots

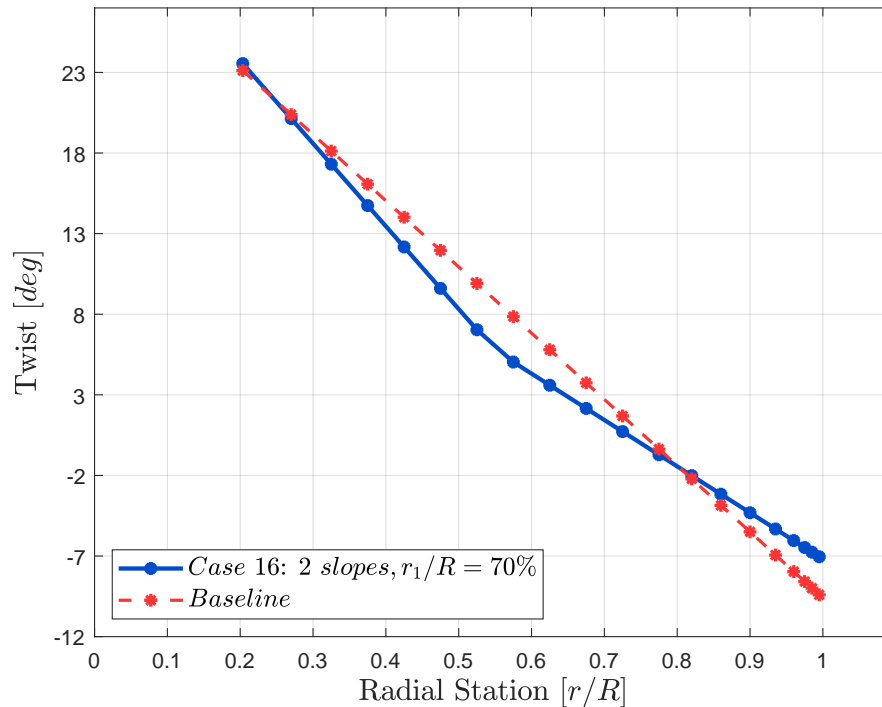


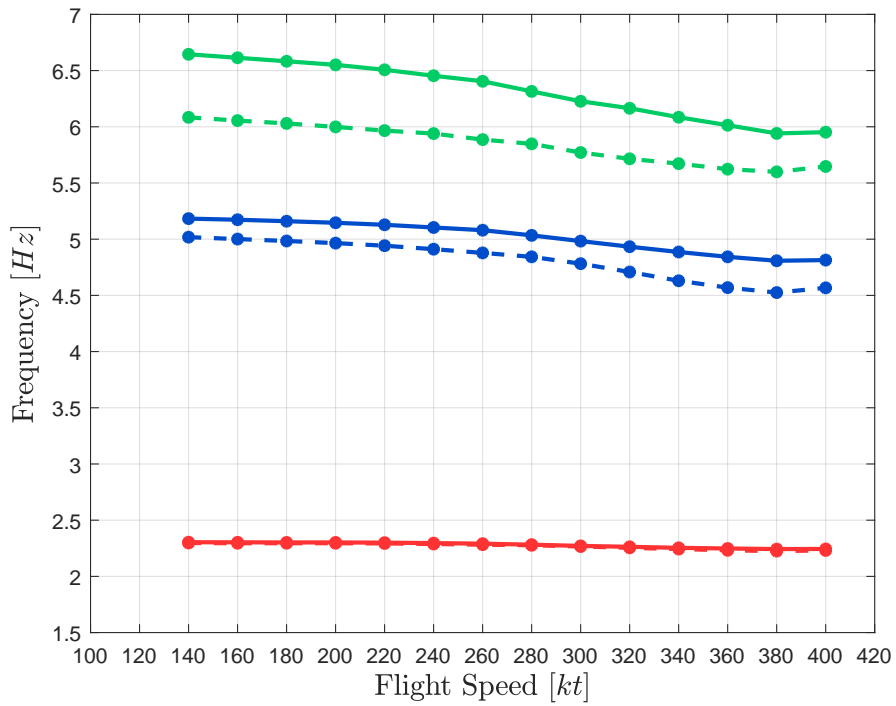
Figure 4.8: Solution 16 - Twist distribution

values in the blade twist, increases the stability for SWC mode, but decreases the AWB and SWT damping for higher velocity. So, the SWC stability limit is shifted, changing the critical mode to the SWT, that drastically decreases for higher velocity.

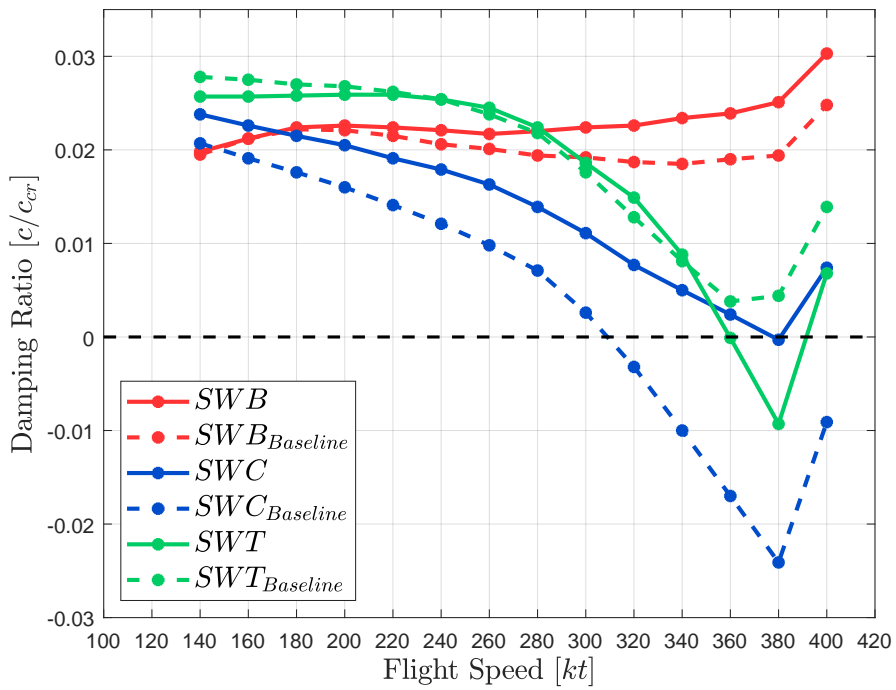
### 4.3.3 Three slope case

The best solution for the three segments case, is the case 21. All the details of this optimization are summarized in the **Table 4.5**. Whirl flutter velocity increases by the 18, 52% using 99, 95% of available power. **Figure 4.11** report the twist distribution of this solution, that shown a similar behaviour of the two slope case, an increase in slope near the root and a reduction near the tip, but less pronounced.

Also in this case the critical modes are the SWC, SWT and AWB, but as seen in **Figures 4.12 4.13**, the SWC drive instability in the symmetric part and AWB in the antisymmetric. Respect to two segments solution, the slope variations in this case are smaller, and the effects are reported in the behaviour of whirl-modes. The change of twist shift the stability for SWC, increasing the limit imposed only by the thickness increase, but decreasing the damping in SWT and AWB.

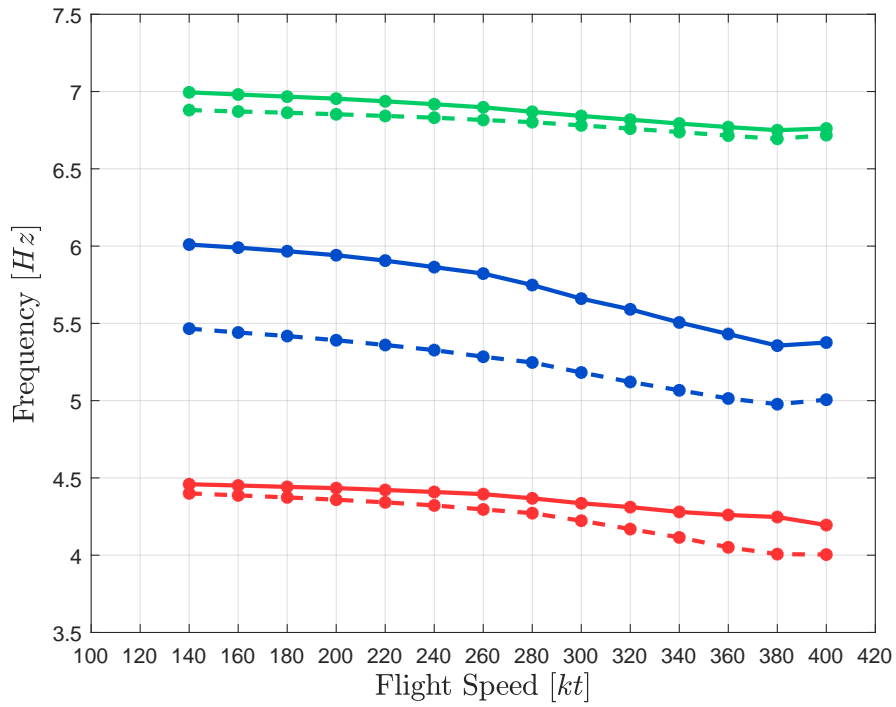


(a) Frequency

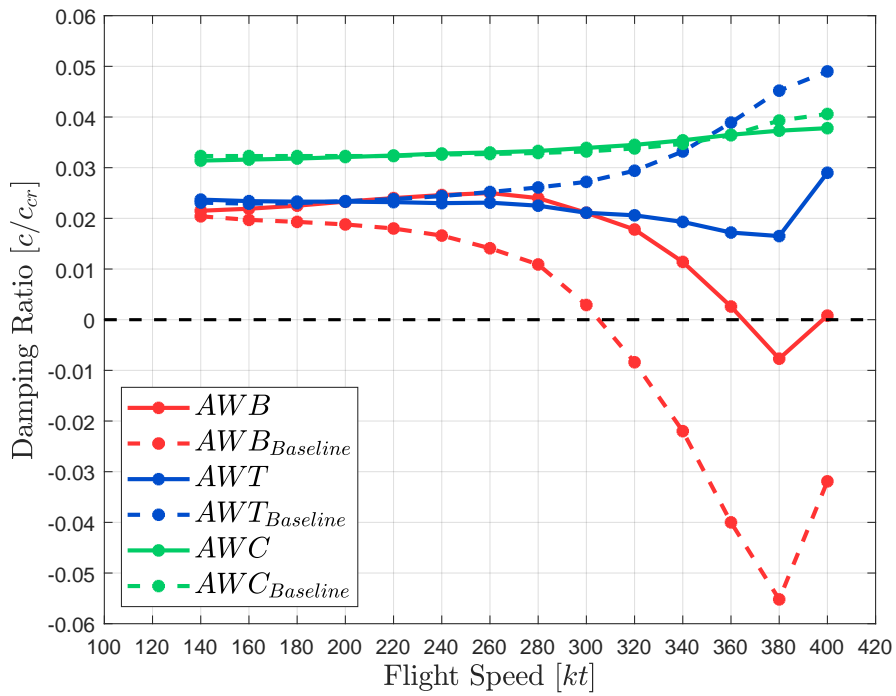


(b) Damping

Figure 4.9: Solution 16: Whirl-mode frequency and damping w.r.t. flight speed - Symmetric roots



(a) Frequency



(b) Damping

Figure 4.10: Solution 16: Whirl-mode frequency and damping w.r.t. flight speed - Antisymmetric roots

Table 4.5: Sol 21 - results summary

Characteristics	Symbols	Values	Units
Thick to chord ratio	$t/c$	0.1726	—
Twist slope ratio - First segment	$\theta_{tw_1}/\theta_{tw_0}$	1.1748	—
Twist slope ratio - Second segment	$\theta_{tw_2}/\theta_{tw_0}$	0.9711	—
Twist slope ratio - Third segment	$\theta_{tw_3}/\theta_{tw_0}$	0.926	—
First slope change radial station	$[r/R]$	40%	—
Second slope change radial station	$[r/R]$	48%	—
Whirl flutter velocity	$V_{wf}$	361,74	$kt$
Power	$P(V_m)$	944,44	$Hp$

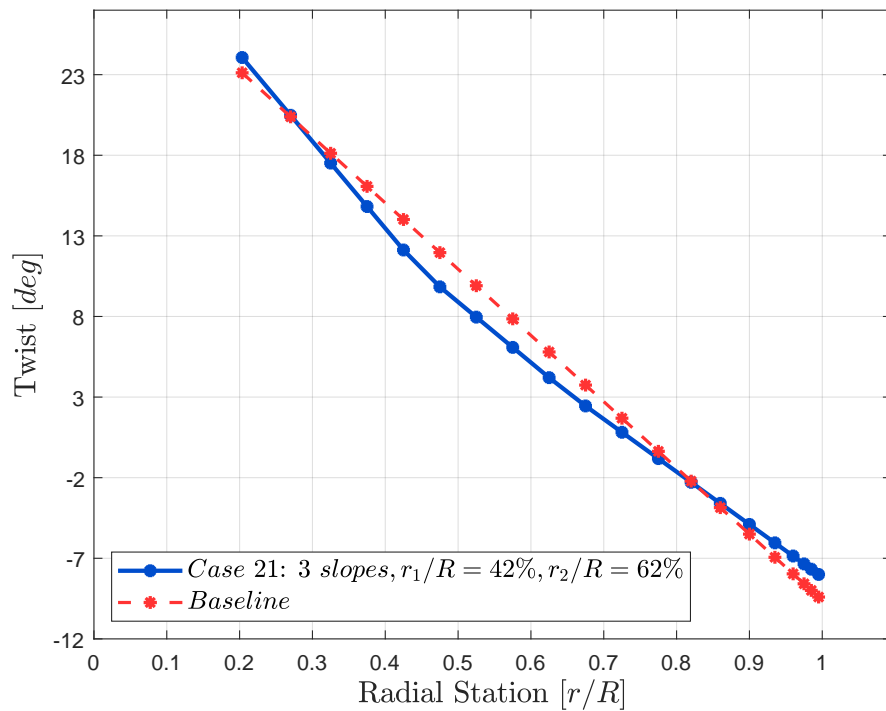
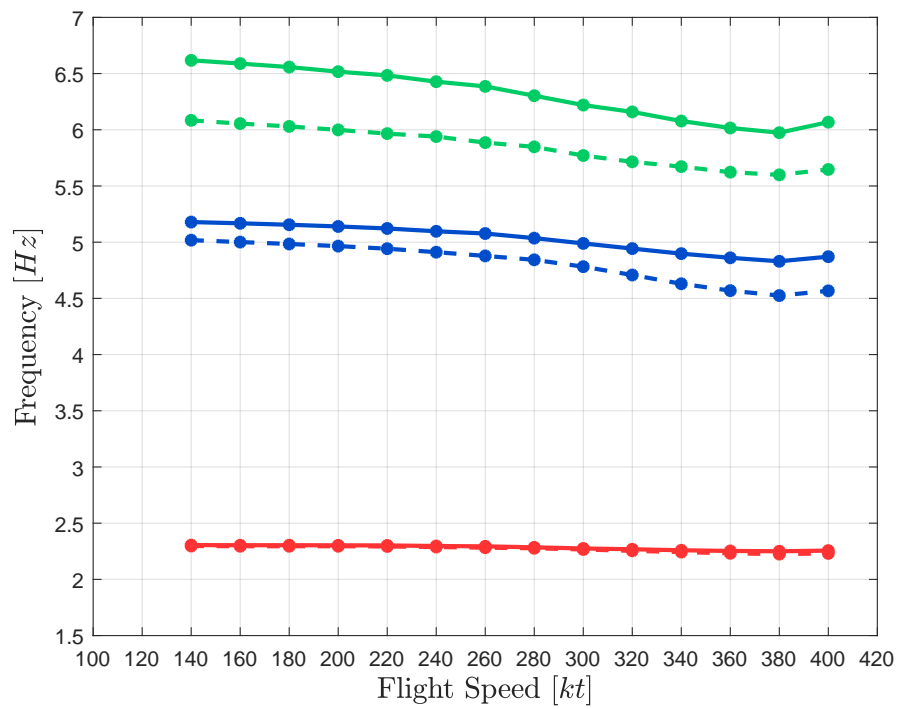
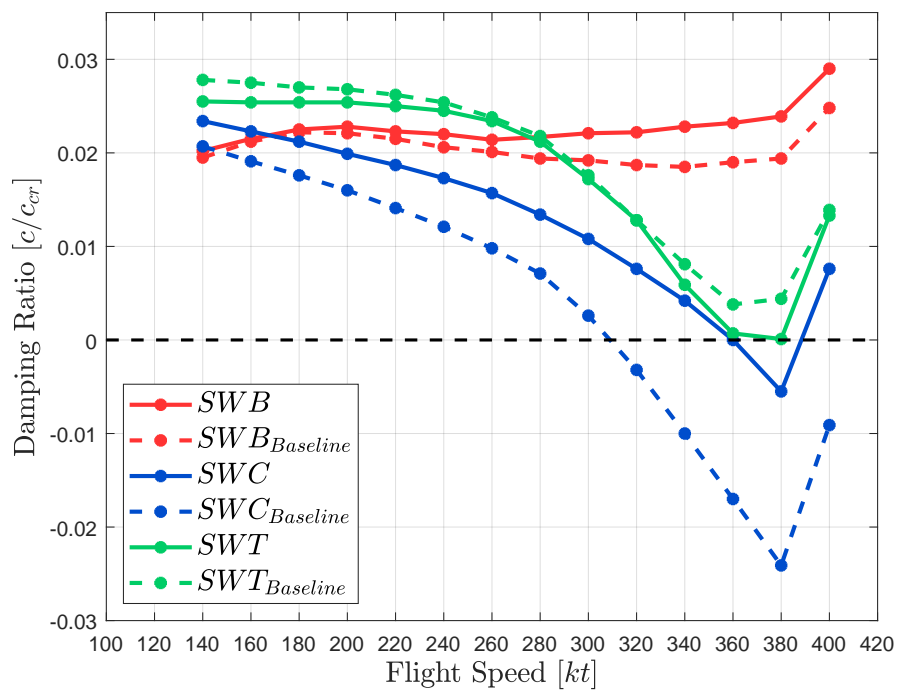


Figure 4.11: Solution 21 - Twist distribution





(a) Frequency



(b) Damping

Figure 4.12: Solution 21: Whirl-mode frequency and damping w.r.t. flight speed - Symmetric roots

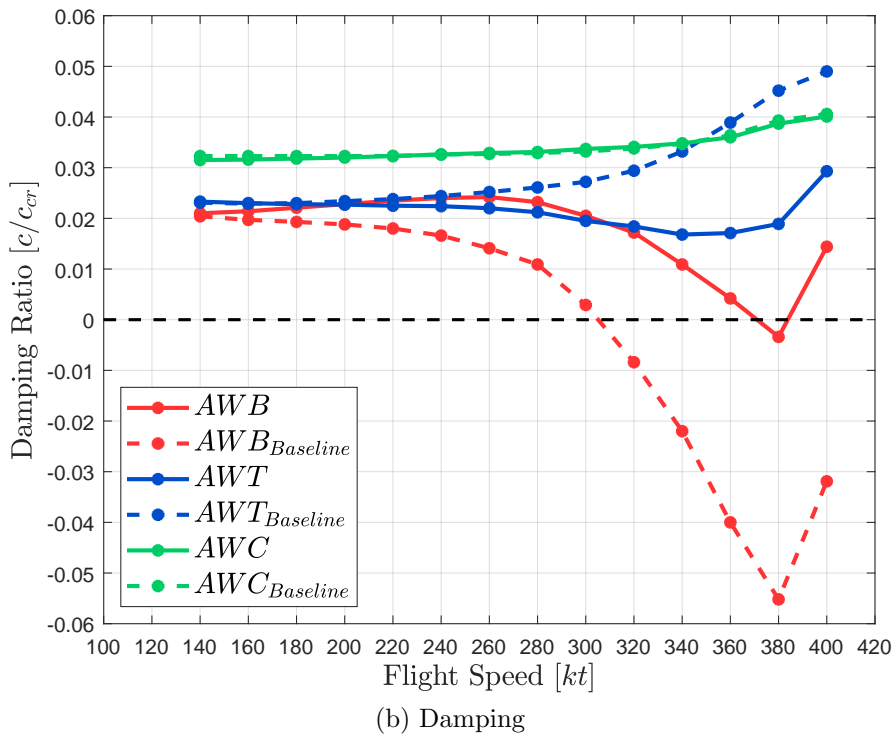
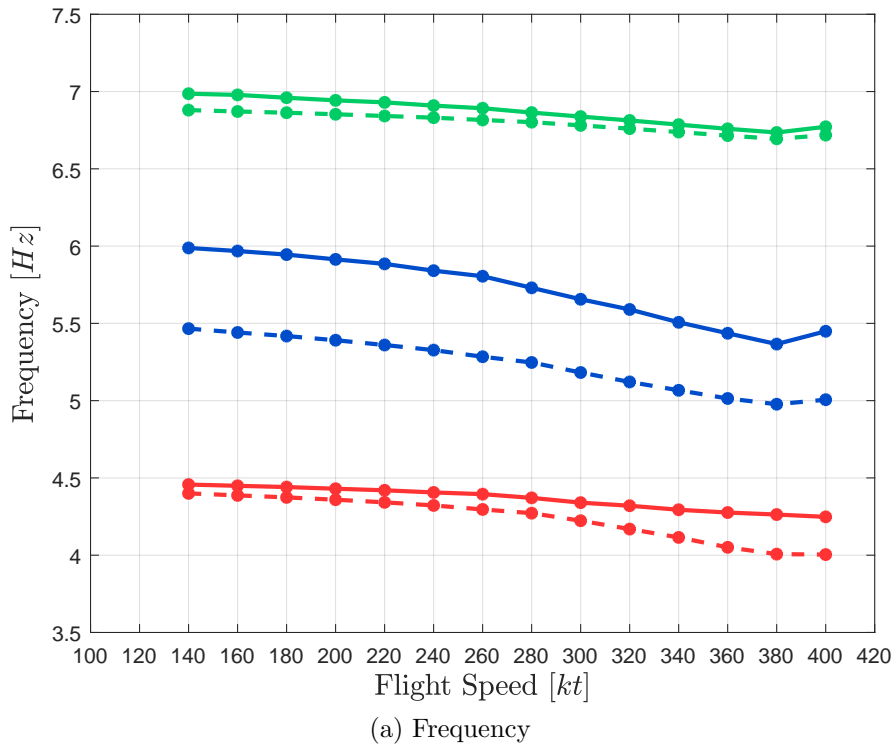


Figure 4.13: Solution 21: Whirl-mode frequency and damping w.r.t. flight speed - Antisymmetric roots

### 4.3.4 Trim and Loads

Comparisons of the trim results with respect to the baseline solution are shown in **Figure 4.14**. For each solution the results are quite similar: power, thanks to the constraints is always lower than the baseline, the same could be said for collective pitch. Thrust is slightly increased due to the wing thickness augmentation, and the pitch attitude for all the cases decrease a little bit respect the baseline.

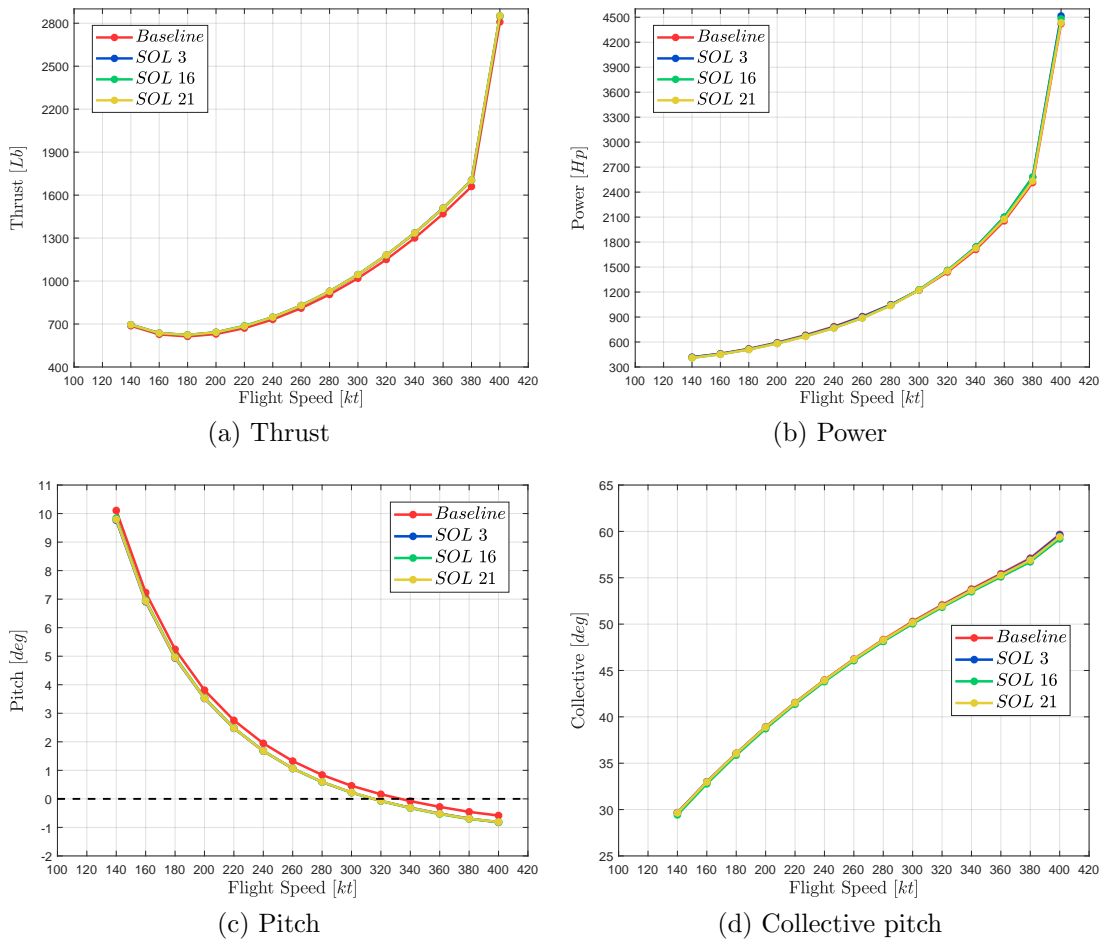


Figure 4.14: Trim results

As mentioned before, the twist modification shift the total thrust toward the blade tip, in particular for the two segment solution, where the twist modification are more important. The shift of thrust increase the bending moment at the blade root and the trim elastic coning angle, that generates an higher positive pitch-lag coupling, generating the stabilizing effect on whirl flutter. The thrust along the blade at 300 kt and the coning angle variation along the flight speed range can be seen in **Figure 4.15**

The new design of the blade must take into account values of the load introduced

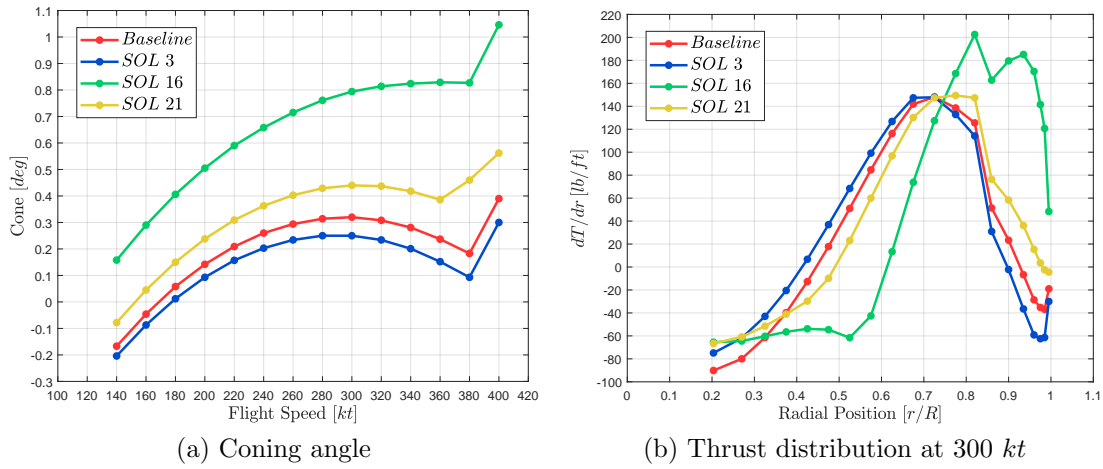


Figure 4.15: Rotor loads and coning angle

by the new configuration. Flapwise bending moment, for example, increase along all the flight envelope for solutions with decreasing slope, moment value at blade root is reported in **Figure 4.16a**. Interesting is the changing produced in the control moment: it decrease for all the velocity, decreasing the impact on rotor pitch link, see **Figure 4.16b** for the trend along flight envelope.

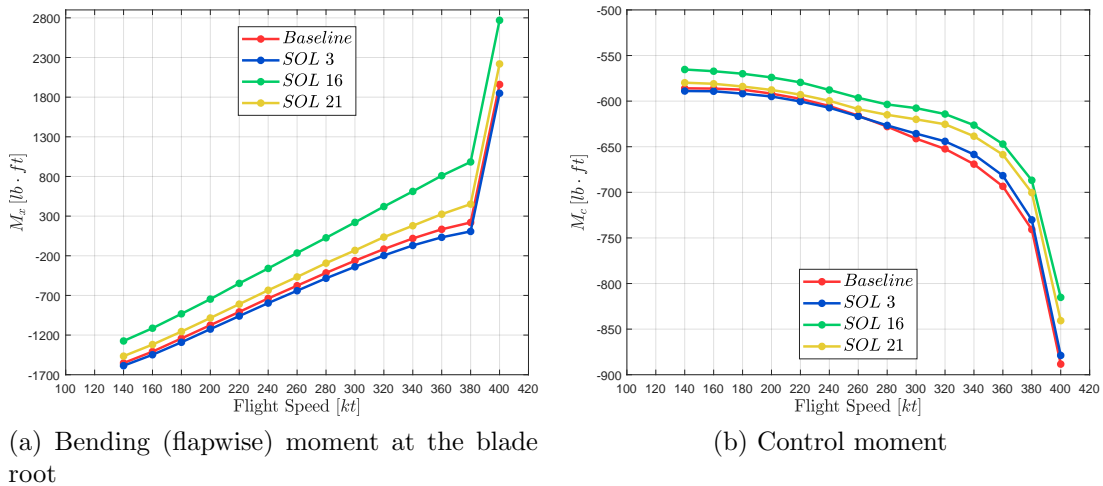


Figure 4.16: Bending and Control moments (mean component) w.r.t. flight speed

## 4.4 Power limitation

Unlimited power represent an ideal condition useful to obtain possible results, but following the aim of thesis, the whirl flutter stability limit need to be increased using a trade off between wing thickness and variation on blade twist law, without changing power-plant of the original aircraft. So in this section, the proposed approach is to make stability analysis on the optimal solutions imposing a trim condition where the power is set to the maximum power supplied by the engine. From Ref.[7], the original XV-15 power-plant is composed by two Lycoming LTC1K-41K turboshaft engines; the details about power rating are listed in **Table 4.6**.

Table 4.6: Lycoming LTC1K-41K turboshaft engine (modified T53L13B) - Power ratings

Horsepower ratings	[SHP]
Contingency (2 minutes)	1802
Takeoff (10 minutes)	1550
Normal (max. continuous)	1250

So from the previous results, up to 300 kt the power required is less than the maximum available power (1250 Hp), after this velocity it has to be imposed the limit on power, modifying in CAMRAD/JA input file the parameters for trim analysis. In this way, an attempt is made to force the aircraft to begin the dive when maximum power limit is reached, in order to obtain the velocity required for the analysis, and thus study its behaviour.

Flutter stability analysis, obviously up to 300 *kt* does not produce any difference between the previous results, but when the aircraft starts to dive, the whirl modes have some variation, in fact the new trim condition generates different instability limit respect the unlimited power case. **Table 4.7**, show the new values of whirl flutter velocity respect previous results.

Table 4.7: Stability limit - Unlimited power w.r.t. Fixed Power

Solution	Whirl flutter velocity [kt]	
	Unlimited	Fixed
One slope	355,22	351.38
Two slopes	359.78	≈ 350
Three slopes	361.74	346.13

With respect to the unlimited power case the critical modes are always the SWC and SWT for symmetric part and AWB in the antisymmetric. The behaviour of

the SWT mode is interesting, because it becomes unstable also in the baseline case, while the other modes do not present noteworthy modifications. **Figure 4.17** show the behaviour of whirl-modes for the one slope solution, in fixed power trim condition. Respect the unlimited power case, the unstable mode that drive instability is the same, SWC, but also the SWT mode becomes unstable following the behaviour of the reference case. However the new trim condition does not change the final value of whirl flutter stability limit.

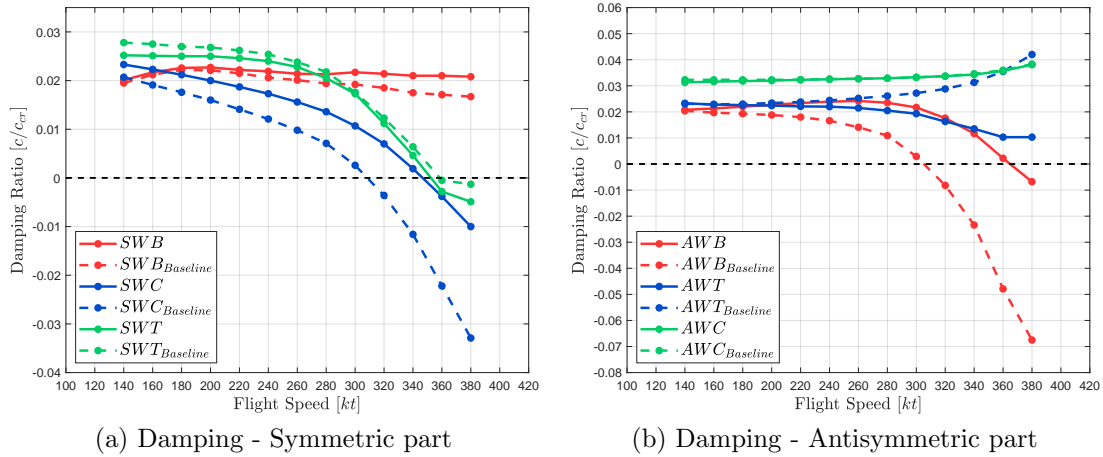


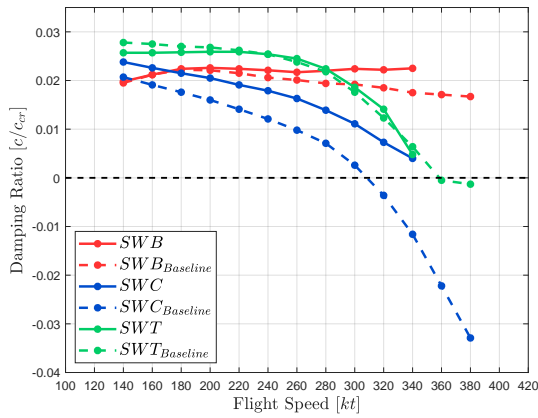
Figure 4.17: One slope Solution : whirl-mode damping w.r.t. flight speed - Fixed power

The two slopes solution have some problem, because above 340 *kt*, CAMRAD/JA is not able to complete the trim analysis, so up to this velocity all modes are stable, but following the behaviour in **Figure 4.18** the instability is close to the final value of the analysis.

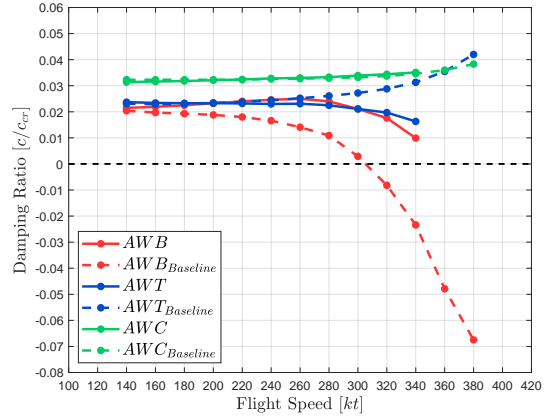
Damping behaviour for the three slopes solution is shown in **Figure 4.19**. Respect to the unlimited power case, the new trim condition decreases the SWT damping, therefore since the SWT mode is the responsible of instability in the unlimited power case, the stability limit can only worsen.

Flutter analysis in fixed power trim condition produce unexpected results, because the solutions that in previous analysis produced the best results, in this case are strongly penalized by reduction in the SWT stability, consequently the relative whirl flutter velocity decrease. From the performance point of view, the aircraft trimmed in dive condition produces some changes, principal results are presented in **Figure 4.20**.

When the aircraft starts to dive, the power is set to the maximum available value, the thrust decrease with the velocity, pitch angle follow the value of climb angle, that becomes negative when the aircraft starts to dive. Finally, the value of collective pitch and the figure of merit are quite similar to the case of unlimited power.

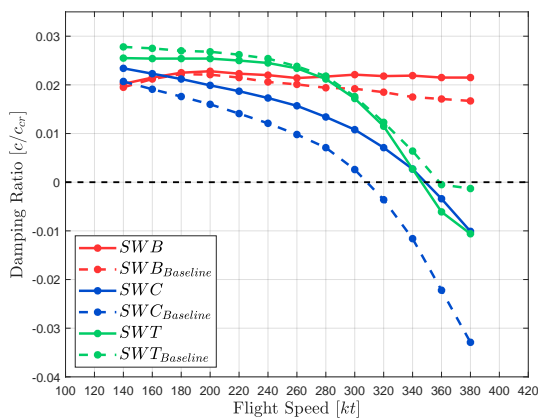


(a) Damping - Symmetric part

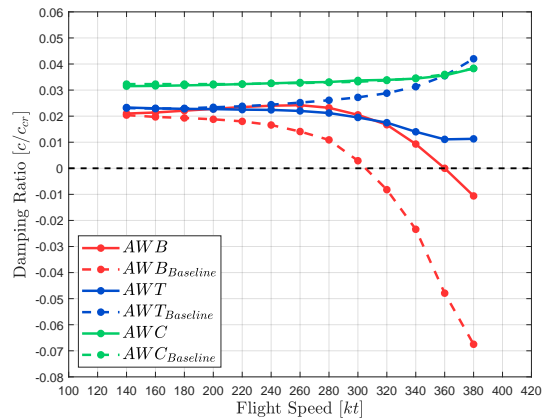


(b) Damping - Antisymmetric part

Figure 4.18: Two slopes Solution : whirl-mode damping w.r.t. flight speed - Fixed power

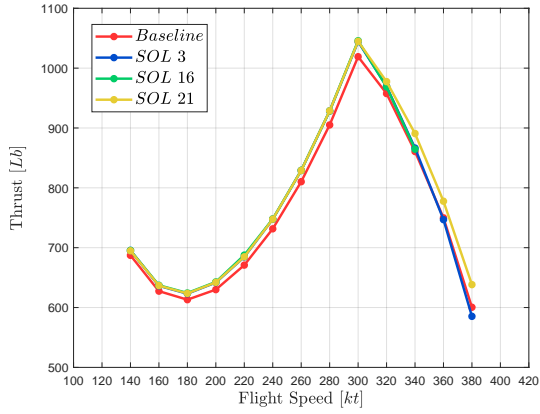


(a) Damping - Symmetric part

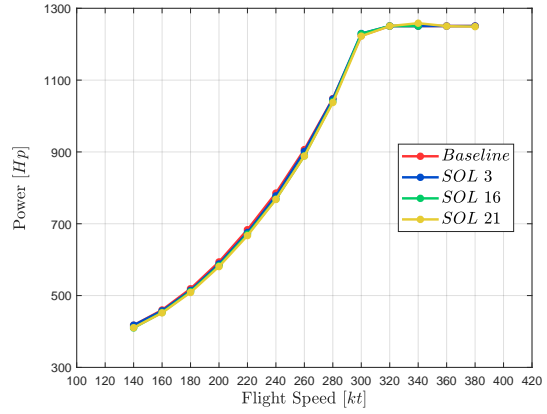


(b) Damping - Antisymmetric part

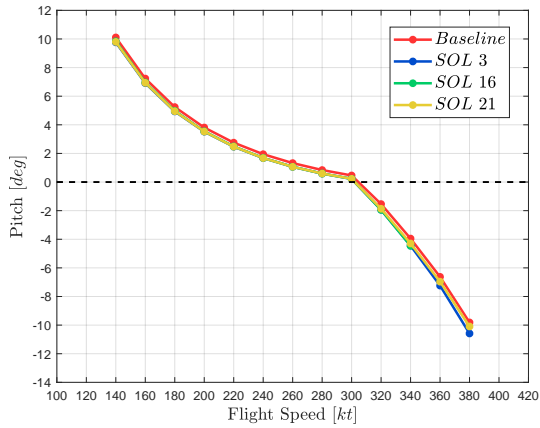
Figure 4.19: Three slopes Solution : whirl-mode damping w.r.t. flight speed - Fixed power



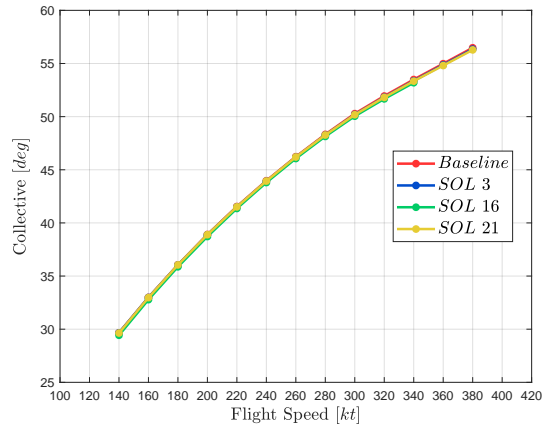
(a) Thrust



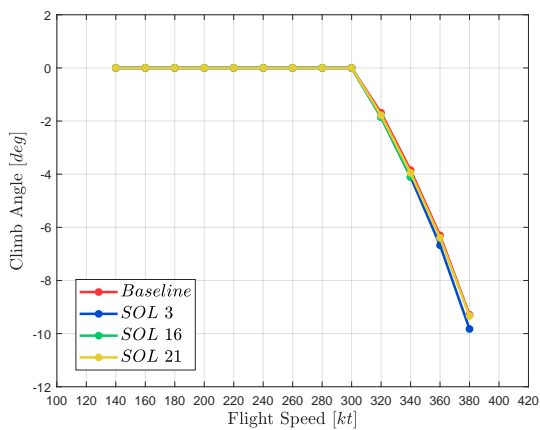
(b) Power



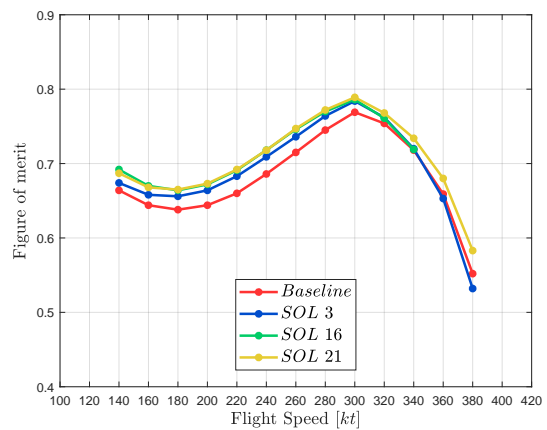
(c) Pitch



(d) Collective pitch



(e) Climb angle



(f) Figure of merit

Figure 4.20: Trim results - Fixed power



The effects of blade twist is also evident in power fixed analysis, because instead the coning angle decrease when the aircraft dives, due to the lower value of thrust, the mean value for the configurations with decreasing slope is always higher than the reference case, as shown in **Figure 4.21a**. The same reasoning can be made also for the bending moment at the blade root (**Figure 4.22a**). Interesting is the behaviour of control moment (**Figure 4.22b**), that respect the unlimited power trim case, mean values are less, in particular the configurations with decreasing slope, in the high velocity range. **Figure 4.21b** shows the thrust distribution along the blade, this time at a speed of 320 kt, the speed in which the aircraft has already started the diving, but despite this, it has the same characteristics as the unlimited power distribution: the solutions with decreasing slopes, they show a trend of the thrust towards the blade tip, vice versa for the single slope case.

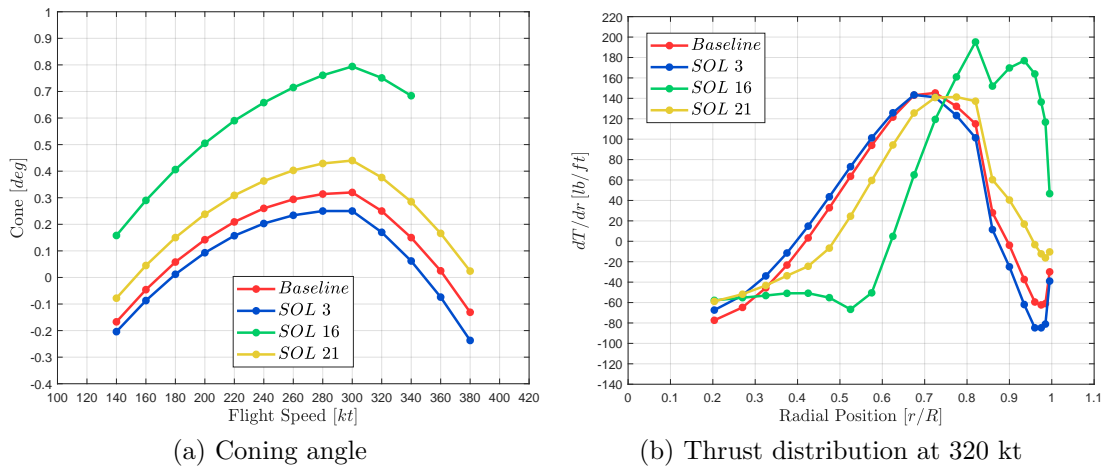


Figure 4.21: Rotor loads and coning angle - Fixed power

In conclusion, the fixed power trim analysis show that the optimal solutions with the best whirl flutter velocity in the unlimited power case, in a more realistic trim configuration does not replicate the same stability margin, but despite this reduction the increase in whirl flutter limit is noteworthy.

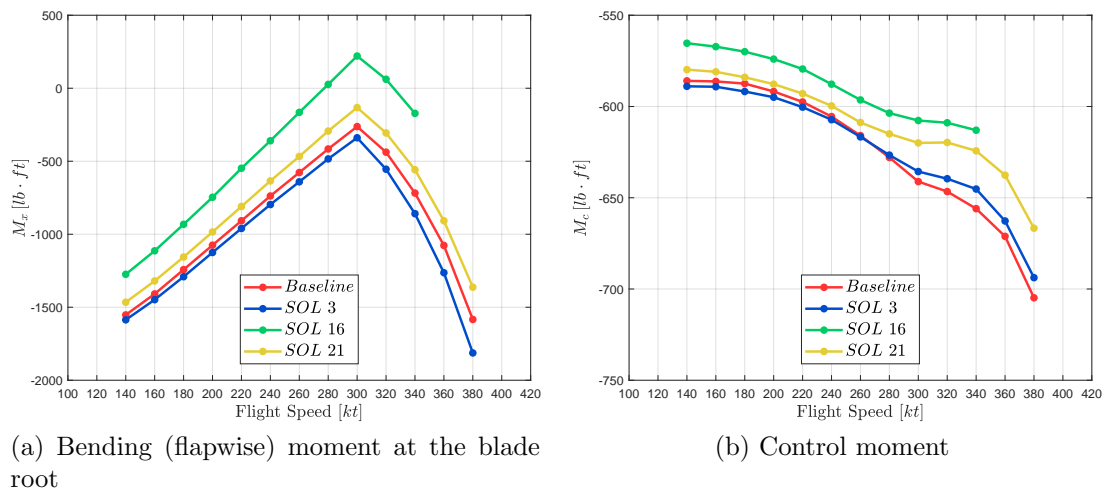


Figure 4.22: Bending and Control moments (mean component) w.r.t. flight speed  
- Fixed power

## 4.5 HEMODE Analysis

For this kind of aircraft the helicopter mode is also important, since it allows the vertical take-off and the possibility of hover condition. So, to analyse how the modification in wing structure and blade twist change the aircraft performance is important. First of all, it is necessary to modify the MSC NASTRAN model in order to compute the modes in HEMODE, configuration with nacelle perpendicular to the wing. After this, CAMRAD/JA settings have been modified in order to consider the aircraft in HEMODE mode, the rotor angular speed is set to 601 rpm and the orientation of the nacelle is changed. The performance analysis is then completed from 0 up to 80 kt, maximum speed for the HEMODE configuration [7].

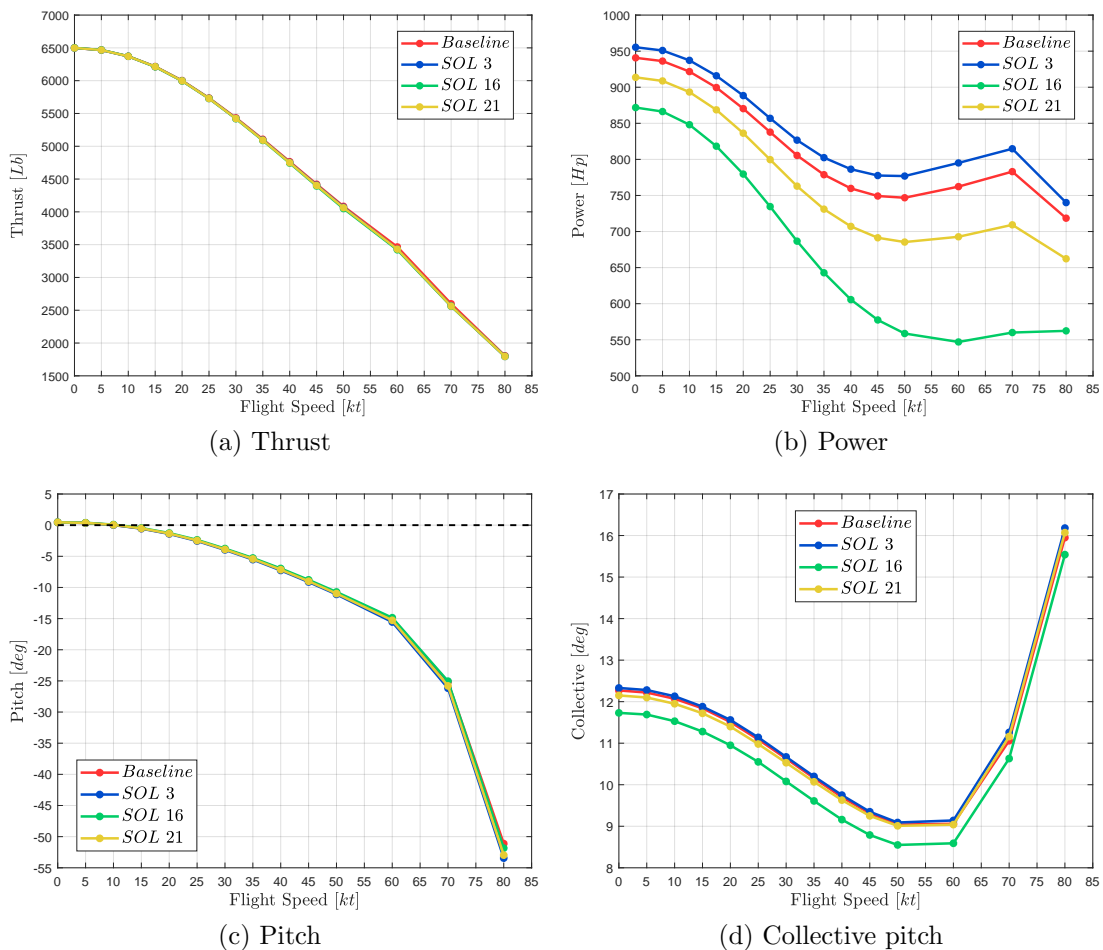


Figure 4.23: HEMODE - Trim results

Trim results are shown in **Figure 4.24**. Respect the baseline configuration, thrust and pitch attitude are quite similar for all the optimal solution, differently for the

power and collective pitch. The power required in the hovering case is lower for the solutions that have a reduced slope in the blade tip, this because the blade configuration is close to an ideal distribution, and remains lower out of the hovering. Furthermore, the blade modifications change the required collective pitch, decreasing it for all the flight condition, especially for the two slopes solution where the twist change are more evident with respect to the baseline. As seen for the APMODE, the modification of the blade twist changes the blade thrust distribution, modifying also the rotor coning angle  $\beta_{trim}$ .

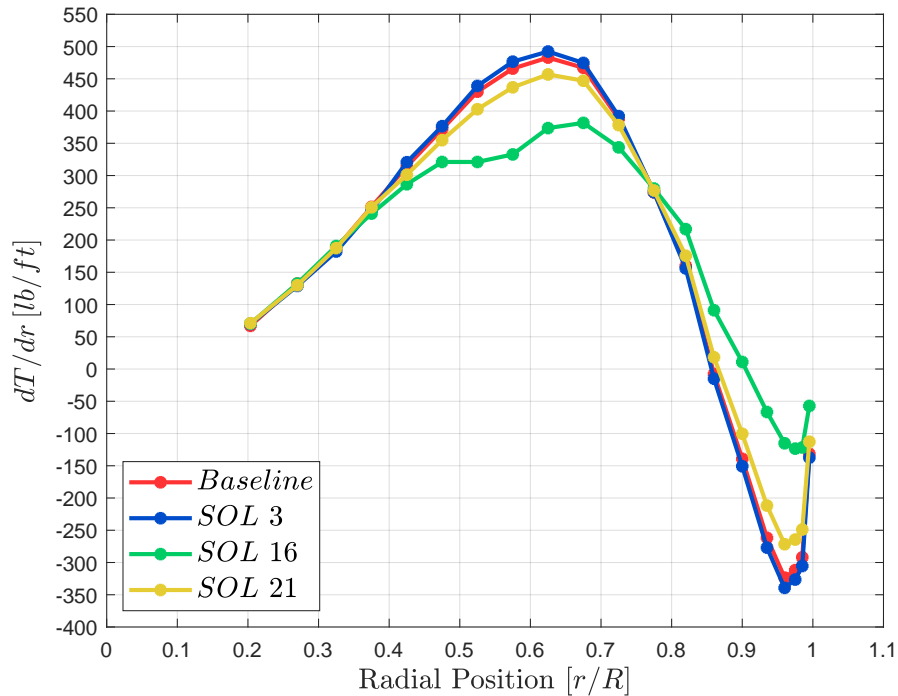


Figure 4.24: HEMODE - Thrust distribution in hovering

Analysing the behaviour in **Figure 4.24**, the thrust distribution in hovering reflect the behaviour of ARMODE, for the solutions with decreasing slope near the tip, the thrust is shifted toward the tip, consequently increase the bending moment at the blade root and the trim coning angle (**Figure 4.25**).

Other interesting parameters are the control moment(**Figure 4.26b**) and the figure of merit (**Figure 4.26a**). As seen for the previous parameters, the trend is similar to the ARMODE, in fact the required control moment decreases along all the velocity range for the increasing twist solutions, and increases a little bit for the one slope solution. Figure of merit (FM), is an Important parameter for helicopter rotor, the solutions with decreasing twist in the blade tip increases the FM value, so the rotor hovering performance are improved. This is good, but higher FM means also higher disk load and this must be taken into account in the rotor design. Increasing the speed, figure of merit collapses, indicating that the configuration with vertical nacelles is not optimal for the forward flight, in fact

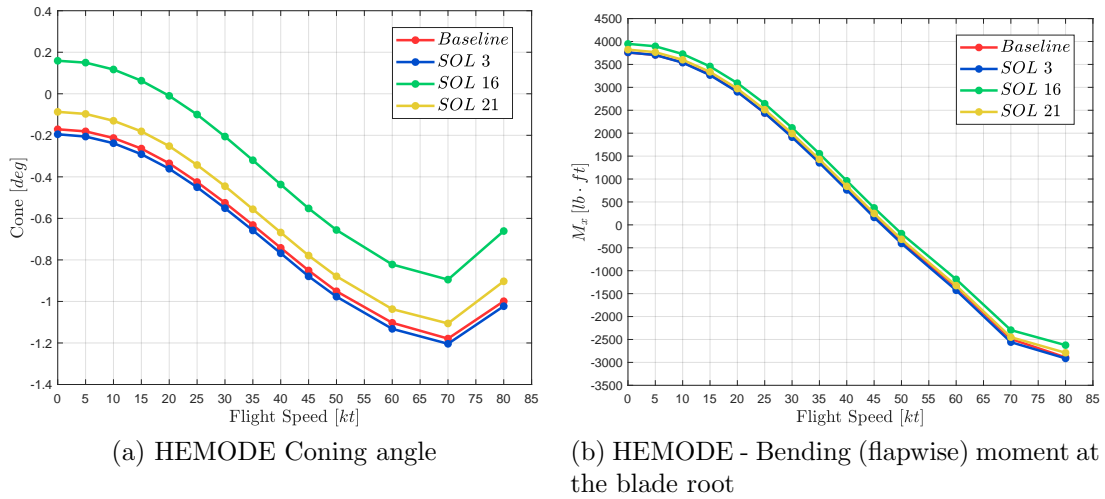


Figure 4.25: HEMODE - Coning angle and Bending moment (mean component) w.r.t. flight speed

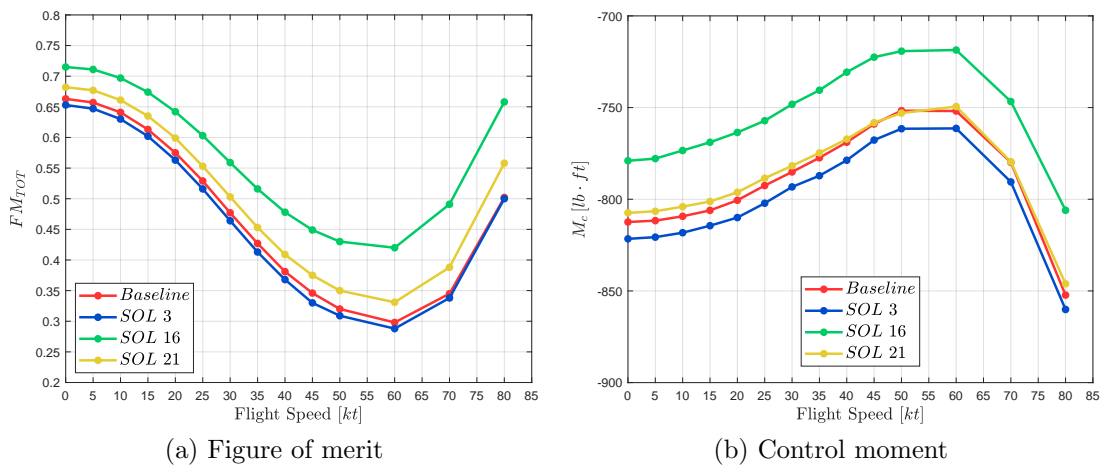


Figure 4.26: HEMODE - Control moment (mean component) and Figure of merit w.r.t. flight speed

when the wing generates enough lift, tilt-rotor starts the configuration change by rotating the nacelle. So blade twist modification, respect the ARMODE, produce similar effects in terms of load and trim parameter; the global efficiency was improved but in the rotor structure must be take into account the increase in loads. In conclusion, it can be said that the changes made to increase the whirl flutter speed, do not go to penalize excessively what are the performances in helicopter mode.

# Conclusions

Detailed aeroelastic tilt-rotor model, based on the real XV-15 aircraft, was analyzed to study an optimal solution to increase the whirl flutter velocity, acting on the rotor blade twist law and on the wing thickness, maintaining the original power plant of the aircraft.

Modal and aerodynamic analysis have been performed on the model in order to evaluate the effects of wing thickness variation. For the optimization procedure, reference case is the model with  $t/c = 0.15$ , in order to better reveal the effects of thickness and blade twist variations. The first effect introduced by the optimization is the tendency to increase the thickness value near  $t/c = 0.17$ , this modify the value of torsional stiffness of the wing, increasing the stability limit of whirl-modes. For the optimization, rotor blade is divided in different segments, one to three, in order to obtain different slope changes on the twist law for the same blade structure. Based on this, the optimization generate different solutions for each case, but only the best solution in terms of whirl flutter velocity is taken into account for a comparison between the different approaches. Each solution generates an increase of 16% or more in the whirl flutter velocity, maintaining the required power below the reference case. Generally, for all solutions, the trend is to increase the wing thickness up to  $t/c \approx 0.173$  and find a trade off with the blade twist in order to satisfy the power constraints and improve the stability requirements. For the solutions with two and three segments, the blade twist slope decreases near the tip and increase in the blade root. The decreasing slope, causes the shift of the total thrust near the tip, increasing the bending moment and the trim coning angle  $\beta_{trim}$ . Another effect is the decrease of the mean component of control moment. For solution with only one segment, in order to decrease the required power due to the thickness, blade twist slope increases along all the blade, generating the opposite effects on the rotor loads.

After this optimization, in order to better evaluate the results, a trim analysis at fixed power has been done. Using the real value of XV-15 power plant, each solution to reach higher velocity starts to dive in a range near 300 kt. This new attitude, change the stability limits, in particular for the SWT mode, reducing the whirl flutter velocity for the solutions with multiple segments. So in this particular trim condition each solution is able to increase the whirl flutter velocity up to  $V_{WF} \approx 350$  kt, value higher with respect to the 305 kt of baseline solution. Loads

in this trim condition reflect the same behaviour seen in the results obtained before. The solutions with multiple segments have loads higher and lower control moment with respect to the baseline and vice versa for the one slope solution.

Finally each solution has been tested in HEMODE, to see the effects of blade twist modification in this configuration. The optimal solutions, as expected, presents a similar behaviour of previous analysis: the twist modification shift the total thrust toward the tip, generating higher bending moment and trim coning angle  $\beta_{trim}$ , decreasing at the same time the mean required control moment. Multiple segments solutions reduce power throughout the analysed flight envelope, in particular the two slope solution where the decrease in blade twist is higher. The obtained results in the HEMODE, shown that the modification made on the blade twist, do not generate significant penalties in the aircraft performances in this configuration.

Future development should add the structural design of the blades considering the effect generated by the different flap bending moments. In conclusion, it was showed that exploiting blade twist it is possible to find the best thickness configuration that expands the flutter free envelope while keeping the power required limited.



# Bibliography

- [1] C. W. Jr. Acree, R. J. Peyran, and W. Johnson. *Rotor Design Options for Improving XV-15 Whirl-Flutter Stability Margins*. Technical Publication. Ames Research Center, Moffett Field, CA 94035-1000.
- [2] C.W. Acree, R.J. Jr Peyran, and W. Johnson. “Rotor Design for Whirl Flutter: An Examination of Options for Improving Tiltrotor Aeroelastic Stability Margins”. In: *American Helicopter Society 55th Annual Forum* (1999).
- [3] Johannes M. van Aken. *Alleviation of Whirl-Flutter on Tilt-Rotor Aircraft Using Active Controls*. Ed. by 47th Forum of the American Helicopter Society. 2 vols. Phoenix, Arizona. 1321 - 1344.
- [4] J. A. Detore and T. M. Gaffey. “The Stopped-Rotor Variant of the Proprotor VTOL Aircraft”. In: *Journal of the American Helicopter Society* 15.3 (), pp. 45–56.
- [5] S. W. Ferguson. *A Mathematical Model for Real Time Flight Simulation of a Generic Tilt-Rotor Aircraft*. Contractor Report CR-166536. NASA, 1988.
- [6] The MathWorks inc. *Constrained Nonlinear Optimization Algorithms*. Matlab Documentation, 2019.
- [7] Giulianetti D. J. Maisel M. D. and Dugan D. C. *The History of the XV-15 Tilt Rotor Research Aircraft: From Concept to Flight*. The NASA History Series. Washington, D.C., 2000.
- [8] D. Matuska, A. Sacullo, and K. Studebaker, eds. *Reduce Tip Speed Testing of a Variable Diameter Tiltrotor Aircraft*. 19th European Rotorcraft Forum. Cernobbio(Como), Italy.
- [9] V. Muscarello and G. Quaranta. *Optimization of Tiltrotor Blade Twist to Increase Whirl-Flutter Stability*. Technical Publication. Politecnico di Milano, 2017.
- [10] M.W. Nixon et al., eds. *Aeroelastic Tailoring for Stability Augmentation and Performance Enhancements of Tiltrotor Aircraft*. NASA Langley Research Center’s International Forum on Aeroelasticity and Structural Dynamics. Williamsburg, Virginia, pp. 121–138.

- [11] D. Popelka et al. “Results of an Aeroelastic Tailoring Study for a Composite Tiltrotor Wing”. In: *51st Annual Forum of the American Helicopter Society* (), pp. 1117–1137.
- [12] H. Reed. *Review Of Propeller-Rotor Whirl Flutter*. Technical report. Langley Station, Hampton, Va.: Langley Research Center.
- [13] V. Srinivas, I. Chopra, and M. W. Nixon. “Aeroelastic Analysis of Advanced Geometry Tiltrotor Aircraft”. In: *Journal of the American Helicopter Society* 43.3 (), pp. 45–56.